Cell Communication and Signaling

RESEARCH Open Access

Concomitant targeting of FLT3 and SPHK1 exerts synergistic cytotoxicity in FLT3-ITD$^+$ acute myeloid leukemia by inhibiting β-catenin activity via the PP2A-GSK3β axis

Ling Jiang[1], Yu Zhao[1,2], Fang Liu[1], Yun Huang[1], Yujiao Zhang[1], Baoyi Yuan[1], Jiaying Cheng[1], Ping Yan[1], Jinle Ni[1], Yongshuai Jiang[3], Quan Wu[1] and Xuejie Jiang[1*]

Abstract

Background Approximately 25–30% of patients with acute myeloid leukemia (AML) have FMS-like receptor tyrosine kinase-3 (FLT3) mutations that contribute to disease progression and poor prognosis. Prolonged exposure to FLT3 tyrosine kinase inhibitors (TKIs) often results in limited clinical responses due to diverse compensatory survival signals. Therefore, there is an urgent need to elucidate the mechanisms underlying FLT3 TKI resistance. Dysregulated sphingolipid metabolism frequently contributes to cancer progression and a poor therapeutic response. However, its relationship with TKI sensitivity in FLT3-mutated AML remains unknown. Thus, we aimed to assess mechanisms of FLT3 TKI resistance in AML.

Methods We performed lipidomics profiling, RNA-seq, qRT-PCR, and enzyme-linked immunosorbent assays to determine potential drivers of sorafenib resistance. FLT3 signaling was inhibited by sorafenib or quizartinib, and SPHK1 was inhibited by using an antagonist or via knockdown. Cell growth and apoptosis were assessed in FLT3-mutated and wild-type AML cell lines via Cell counting kit-8, PI staining, and Annexin-V/7AAD assays. Western blotting and immunofluorescence assays were employed to explore the underlying molecular mechanisms through rescue experiments using SPHK1 overexpression and exogenous S1P, as well as inhibitors of S1P2, β-catenin, PP2A, and GSK3β. Xenograft murine model, patient samples, and publicly available data were analyzed to corroborate our *in vitro* results.

Results We demonstrate that long-term sorafenib treatment upregulates SPHK1/sphingosine-1-phosphate (S1P) signaling, which in turn positively modulates β-catenin signaling to counteract TKI-mediated suppression of FLT3-mutated AML cells via the S1P2 receptor. Genetic or pharmacological inhibition of SPHK1 potently enhanced the TKI-mediated inhibition of proliferation and apoptosis induction in FLT3-mutated AML cells in vitro. SPHK1 knockdown enhanced sorafenib efficacy and improved survival of AML-xenografted mice. Mechanistically, targeting the SPHK1/

*Correspondence:
Xuejie Jiang
jxj3331233@163.com

Full list of author information is available at the end of the article

S1P/S1P2 signaling synergizes with FLT3 TKIs to inhibit β-catenin activity by activating the protein phosphatase 2 A (PP2A)-glycogen synthase kinase 3β (GSK3β) pathway.

Conclusions These findings establish the sphingolipid metabolic enzyme SPHK1 as a regulator of TKI sensitivity and suggest that combining SPHK1 inhibition with TKIs could be an effective approach for treating FLT3-mutated AML.

Keywords FLT3, Acute myeloid leukemia, SPHK1, Sphingolipid, Tyrosine kinase inhibitor, B-catenin

Background

Acute myeloid leukemia (AML) is an aggressive hematological malignancy with distinct heterogeneity. Internal tandem duplication (ITD) mutations of the FMS-like receptor tyrosine kinase 3 (FLT3) are among the most frequent mutations, found in 25–30% of patients with AML [1]. These mutations cause ligand-independent phosphorylation of FLT3 and subsequent activation of downstream effectors, which can confer a high risk of relapse and an adverse prognosis [2]. Although FLT3 tyrosine kinase inhibitors (TKIs), such as midostaurin, sorafenib, and gilteritinib, offer clinical benefit to patients with FLT3-mutated AML, their effectiveness is often transient owing to secondary FLT3 mutations and bone marrow microenvironment-mediated resistance [3, 4]. Several studies have suggested that prolonged exposure to FLT3 inhibitors leads to resistance via the activation of parallel pathways that provide compensatory survival signals [5–7]. Therefore, an approach combining FLT3 TKIs with the suppression of important downstream pathways may reduce the chances of developing resistance and ultimately sustain disease remission in FLT3-ITD$^+$ AML patients.

In addition to their role as components of eukaryotic cell membranes, sphingolipids function as bioactive molecules that regulate intracellular physiological and pathological processes [8, 9]. Sphingosine kinase 1 (SPHK1) is a key enzyme in sphingolipid metabolism that phosphorylates sphingosine to generate sphingosine-1-phosphate (S1P) [10], thereby balancing the levels of pro-apoptotic ceramide and pro-survival S1P within cells [11]. Generally, SPHK1/S1P signaling functions through five S1P-specific transmembrane G-protein-coupled receptors, namely S1P1–5 [12]. Activation of SPHK1 and the subsequent generation of S1P are associated with a poor therapeutic response and patient prognosis in various cancers [13–15]. However, the compensatory survival mechanism of SPHK1/S1P signaling following prolonged exposure to FLT3 inhibitors has not been well studied.

Wnt/β-catenin signaling plays essential roles in cell fate determination, tissue development, and disease pathogenesis [16]. Aberrant β-catenin signaling contributes to FLT3-ITD-related leukemic signal transduction [17] and promotes the survival and function of leukemia stem cells (LSCs) [18, 19], which are potential sources of leukemia relapse [20]. We previously demonstrated that inhibiting β-catenin exhibits potential cytotoxicity in FLT3-ITD$^+$ AML cells and LSCs, significantly enhancing the antileukemia efficacy of FLT3 TKIs [21]. Thus, β-catenin inhibition represents a promising strategy for improving TKI sensitivity. In liver cancer, targeting SPHK1 was shown to inhibit cell proliferation by suppressing the Wnt5A/β-catenin pathway [22]. Therefore, we aimed to explore the regulatory effect of SPHK1/S1P on β-catenin signaling and its role in protecting FLT3-ITD$^+$ AML cells against TKI treatment.

In this study, we found that long-term FLT3 inhibition activates the SPHK1/S1P axis in FLT3-ITD$^+$ AML cells. SPHK1 overexpression or exogenous S1P upregulated β-catenin signaling via the S1P2 receptor, protecting leukemia cells against FLT3 TKIs. However, targeting SPHK1 synergized with TKIs to suppress cell growth and induce apoptosis in FLT3-ITD$^+$ AML cells and primary AML samples. The synergistic antileukemic efficacy of this drug combination was mediated via activation of the protein phosphatase 2 A (PP2A)-glycogen synthase kinase 3β (GSK3β) axis, which suppresses the nuclear translocation of pro-survival protein β-catenin. Taken together, we propose that targeting SPHK1/S1P signaling and modulating the PP2A-GSK3β-β-catenin axis could enhance the efficacy of TKIs against FLT3-ITD$^+$ AML.

Methods

Cell lines and reagents

Human FLT3-ITD$^+$ AML cell lines Molm13 and MV4-11, as well as FLT3 wild-type (FLT3-WT) cell lines HL-60 and THP-1, were routinely cultured in RPMI-1640 medium supplemented with 10% fetal bovine serum plus 1% penicillin/streptomycin at 37 ℃ under a humidified atmosphere containing 5% CO_2. Cell lines were authenticated via STR DNA fingerprinting using the AmpFISTR Identifier PCR Amplification Kit (Thermo Fisher Scientific, Waltham, MA, USA) and were routinely tested for mycoplasma using the PCR Mycoplasma Detection Kit (Vazyme, Nanjing, China).

Sorafenib (Cat. No. HY-10201), quizartinib (Cat. No. HY-13001), S1P (Cat. No. HY-108496), SKI-II (Cat. No. HY-13822, SPHK inhibitor), MSAB (Cat. No. HY-120697, β-catenin inhibitor), JTE-013 (Cat. No. HY-100675, S1P2 inhibitor), okadaic acid (Cat. No. HY-N6785, PP2A inhibitor), and TWS-119 (Cat. No. HY-10590, GSK3β

inhibitor) were purchased from MedChemExpress (Monmouth Junction, NJ, USA).

Primary AML samples

Bone marrow (BM) samples were collected from AML patients and healthy donors after obtaining informed consent following approval by the Medical Ethics Committee of Nanfang Hospital, in compliance with the Declaration of Helsinki. Mononuclear blasts were purified via density gradient centrifugation over Lymphoprep (TBDsciences, Tianjin, China) and cultured in IMDM with 20% FBS. Table S1 summarizes patient clinical characteristics.

Quantitative reverse transcription-polymerase chain reaction (qRT-PCR) assay

Total RNA extracted from cells was reverse-transcribed into cDNA using HiScript® III All-in-one RT SuperMix (Vazyme). qRT-PCR was conducted using Taq Pro Universal SYBR qPCR Master Mix (Vazyme) on a QuantStudio™ 5 Real-Time PCR System (Applied Biosystems, Foster City, CA, USA). The primer sequences are listed in Table S2.

RNA-sequencing (RNA-seq)

Molm13 cells treated with DMSO (control) or sorafenib for 3 months were subjected to RNA-seq. Total RNA was isolated using TRIzol® Reagent (Thermo Fisher Scientific). The library was generated using a NEBNext® UltraTM RNA Library Prep Kit for Illumina® (NEBiolabs, Ipswich, MA, USA) and sequenced on an Illumina NovaSeq6000 system (San Diego, CA, USA). Raw sequence reads were first processed using the FastQC (http://www.bioinformatics.Babraham.ac.uk/projects/fastqc/) tool for quality control. Clean reads were obtained by removing adaptor sequences and low-quality reads from raw data. Fastq files were aligned to the human reference genome via HISAT2 (http://daehwankimlab.github.io/hisat2/) software. The R package DESeq2 v1.36.0 was utilized to identify differentially expressed genes. The R package pheatmap v1.0.12 was utilized to generate the heatmap.

Lipidomics analysis via high-performance liquid chromatography-mass spectrometry (HPLC-MS)

Molm3 cells collected 3 months post-sorafenib exposure or untreated cells were subjected to lipidomic profiling analysis (Table S3). Briefly, approximately one million cells were homogenized in 750 μL of chloroform: methanol: MilliQ H2O (3:6:1, v/v/v) and incubated at 1500 rpm for 1 h at 4 ℃. Subsequently, 350 μL of H_2O and 250 μL of chloroform were added, followed by centrifugation to separate the lipid-containing organic phase. Lipid extraction was repeated with 450 μL of chloroform, and extracts were pooled and dried in a SpeedVac (Thermo Fisher Scientific) for LC-MS analysis. The LC-MS analysis was done using a Jasper HPLC coupled with Sciex TRIPLE QUAD 4500 MD (Sciex, Framingham, MA, USA), as previously reported [23]. Chromatographic separation via normal phase-HPLC was performed on a TUP-HB silica column (3 μm, 150 mm ×2.1 mm). Multiple reaction monitoring transitions were set up for the comparative analysis of various lipids. Individual lipid species were quantified via reference to spiked internal standards. D9-PC32:0(16:0/16:0), PE 34:0, dic8-PI, d31-PS, C17:0-PA, DMPG, CL-14:0, C14-BMP, C12-SL, C17-LPC, C17-LPE, C17:1-LPI, C17:0-LPA, C17:1-LPS, C17-Cer, C12-SM, d17:1-S1P, d17:1-Sph, C8-GluCer, C8-LacCer, Gb3-d18:1/17:0, d3-16:0 carnitine, and DAG (18:1/18:1)-d5 were obtained from Avanti Polar Lipids (Alabaster, AL, USA). GM3-d18:1/18:0-d3 was purchased from Matreya LLC (Ann Arbor, MI, USA). Free fatty acids were quantitated using d31-16:0 (Sigma-Aldrich, St. Louis, MO, USA). D6-CE 18:0 and TAG (16:0) 3-d5 were obtained from CDN isotopes (Montreal, Canada).

Bioinformatic analysis of public databases and online search tool

Microarray and RNA-seq data from GEO databases (GSE74666 [24] and GSE168583 [25]) were utilized to plot a heatmap depicting the differential expression of sphingolipid metabolism genes between FLT3-ITD$^+$ AML parental and TKI-resistant cell lines. Based on the Molecular Signatures Database (MSigDB, https://www.gsea-msigdb.org/), gene set enrichment analysis (GSEA) was conducted on GSE74666 to investigate the association between sorafenib resistance and sphingolipid metabolism. RNA-seq data of AML patients were downloaded from The Cancer Genome Atlas (TCGA) database. GSEA was performed to explore the role of SPHK1 in AML pathogenesis. Spearman's correlation analysis was performed to evaluate the relationship between SPHK1 and S1P1–5 expression. CRISPR screen data from The Cancer Dependency Map (DepMap) (https://depmap.org/portal/) database were used to determine if leukemia cells were dependent on SPHK1. To investigate the prognostic value of 16 sphingolipid metabolic genes, S1P2, and β-catenin in AML patients, survival curves were generated and downloaded from the Kaplan–Meier (KM) plotter database (http://kmplot.com/analysis/).

Enzyme-linked immunosorbent assay (ELISA)

For S1P quantification, cell lysates from FLT3-ITD$^+$ AML cell lines and bone marrow supernatant from FLT3-ITD$^+$ AML patients were analyzed using an S1P ELISA Kit (Fine Test Biotech, Wuhan, China), following the manufacturer's protocols.

Growth inhibition assay

AML cell lines (2×10^5 cells/mL) were plated in 96-well plates and treated with the indicated doses of SKI-II (SPHK inhibitor) or FLT3 TKI alone or in combination for 48 h. The cytotoxic effects were measured in triplicate using the Cell Counting Kit-8 (CCK-8) Assay Kit (Dojindo, Japan). Briefly, the CCK-8 solution (10 μL/well) was added to 100 μL of medium containing the drug, followed by an additional 2-h incubation at 37 °C. Absorbance was measured at 450 nm using a microplate reader (Bio-Tek, USA), and cell viability was determined for each group via comparison to the untreated control.

Apoptosis and cell cycle distribution analysis via flow cytometry

AML cell lines (2×10^5 cells/mL) and primary samples (5×10^5 cells/mL) were seeded in 24-well plates with or without bone marrow-derived mesenchymal stem cell co-culture and treated with the indicated concentrations of different drugs for 48 h. Apoptosis was measured by incubating the treated cells with Annexin V-APC/7-AAD (KeyGen) for 10 min, as per manufacturer's instructions. Cell cycle analysis was performed using the Cell Cycle Staining Kit (Multisciences, China) according to the manufacturer's instructions. The cells were incubated with a PI staining solution containing RNase A and a permeabilization solution for 30 min in the dark at 25 °C. Apoptotic assays and cell cycle distribution were performed using a BD FACSCanto instrument (BD Biosciences, San Jose, CA, USA). All data were processed using FlowJo v10.8.1 software (FlowJo, LLC., Ashland, OR, USA).

Western blot analysis

After treatment with different compounds for the indicated times, cell lysates were separated via 10% SDS-PAGE. Proteins were transferred to PVDF membranes (Beyotime, Shanghai, China) and probed with the indicated primary antibodies, followed by horseradish peroxidase-conjugated goat anti-rabbit or anti-mouse secondary antibodies. Signals were detected using an ECL Western Blotting Detection Kit (FudeBio, Hangzhou, China) and visualized on a Chemiluminescent Imaging System (SINSAGE, Beijing, China). Nuclear and cytoplasmic fractions were isolated using a Nuclear and Cytoplasmic Protein Extraction Kit (KeyGEN, Nanjing, China). Antibodies against FLT3 (#3462), phospho (p)-FLT3 (Tyr589/591) (#3464), SPHK1 (#12071), SPHK2 (#32346), GSK3β (#9315), p-GSK3β (Ser9) (#9336), β-catenin (#8480), c-Myc (#5605), Survivin (#2808), CD44 (#5640), caspase-3 (#9662), and PARP (#9532) were obtained from Cell Signaling Technology (CST, Beverly, MA, USA). p-PP2A-Cα/β (Tyr307) (sc-271903) was purchased from Santa Cruz Biotechnology (Dallas, Texas, USA), and PP2A-C subunit (#05-421) was obtained from Millipore (Billerica, MA, USA). GAPDH (#2118), β-tubulin (#2128), and Lamin B1 (#13435) (all from CST) were used as loading controls.

Immunofluorescence staining and confocal microscopy

A total of 1×10^5 cells were cytospun onto glass slides, fixed in 4% paraformaldehyde, permeabilized with 0.2% Triton X-100, and blocked with 10% goat serum. The cells were then stained with rabbit anti-human β-catenin and mouse anti-human CD44 primary antibodies (1:200 dilution; CST), followed by incubation with Alexa Fluor488-conjugated goat anti-rabbit and Alexa Fluor 594-conjugated goat anti-mouse secondary antibodies (1:5000 dilution; Abcam, Cambridge Biomedical Campus, Cambridge, UK). After the nuclei were counterstained with a 4′,6-diamidino-2-phenylindole (DAPI)-containing antifade mountant (Beyotime), nail polish was added to seal the coverslips. Immunofluorescence images were acquired using a Zeiss LSM 980 confocal laser-scanning microscope (Oberkochen, Germany). Images of Molm13 and MV4-11 cells were captured using Plan-Apochromat 63×/1.40 Oil DIC M27 and 40×/0.95 Korr M27 objectives, respectively. Images were loaded into ImageJ v1.48 (National Institutes of Health, Bethesda, MD, USA) software. All channels were utilized to generate the whole cell mask, with DAPI determining the nuclear region. Proteins co-localized with DAPI were regarded as located in the nucleus. The cytoplasmic mask was derived by subtracting the nuclear mask from the whole cell mask. The mean intensity for each of the nuclear, cytoplasmic, and whole cell masks was quantified using ImageJ.

Generation of SPHK1 overexpression or knockdown cell lines

Lentiviral overexpression plasmids carrying human SPHK1 (Accession Number: NM_182965.3) and lentiviral constructs of SPHK1 small hairpin RNA (shRNA) (listed in Table S4) were purchased from the Public Protein/Plasmid Library (Nanjing, China). The pPLK vectors and package plasmids (pMD2.G and psPAX2) were co-transfected into HEK293T cells for lentiviral production, and the virus-containing supernatants were collected. In total, 2×10^5 Molm13 or MV4-11 cells were seeded in 24-well plate in the presence of 10 μg/mL polybrene and centrifuged with lentivirus at MOI 100 at 2000 rpm for 1 h at room temperature. After overnight transduction in the incubator, the medium was replaced, and the cells were cultured for further puromycin selection to achieve stable integration.

AML mouse xenograft model

Animal experiments were approved by the Institutional Animal Ethics Committee of Nanfang Hospital. GFP/Luciferase-labeled Molm13 cells (Molm13-GFP/Luc, 5×10^5) stably expressing either shCtrl or shSPHK1 were transplanted into 6-8-wk-old female NOD/ShiLtJGpt-Prkdcem26/IL2rgem26/Gpt (NCG) mice (GemPharmatech, Guangdong, China) via tail vein injection. After confirming engraftment through bioluminescence imaging, the mice were randomly allocated to four groups ($n=10$/group) and treated with either vehicle or sorafenib (4 mg/kg/day, oral gavage) for 4 weeks. Three mice per group were euthanized on day 14 of the treatment. Spleen and bone marrow samples were stained with human CD45 antibody and analyzed by flow cytometry to assess leukemia burden. The remaining seven mice per group were monitored for survival.

Statistical analyses

Experiments were performed in triplicate, and data were expressed as means±standard error of the mean (SEM). Statistical analyses were performed using GraphPad Prism v8.0 (Graph Pad Inc., San Diego, CA, USA). Combinatorial index (CI) values were calculated via the Chou-Talalay method using Compusyn v1.0 software (ComboSyn, Inc., Paramus, NJ, USA), with CI<1 indicating synergistic, =1 indicating additive, and >1 indicating antagonistic effects. The averaged CI obtained at the effective doses of 50%, 75%, 90%, and 95% were used. Statistical significance was determined using unpaired or paired two-tailed Student's t-tests for the comparison of two groups and one-way analysis of variance (ANOVA) for multiple-group comparisons. Mouse survival was estimated using the Kaplan–Meier method and compared using the log-rank test. $p<0.05$ was considered statistically significant.

Results

Sphingolipid metabolism is dynamically regulated after long-term FLT3 inhibitor exposure

To study the changes in lipid metabolism associated with prolonged exposure to FLT3 inhibitors, we performed lipidomic profiling of human FLT3-ITD$^+$ Molm13 cells after exposure to sorafenib for 3 months using LC-MS (Fig. 1a). In total, 575 metabolites were identified and categorized into four classes based on their lipid backbone. Notably, sphingolipids exhibited the most significant alterations among metabolites, with a predominant increase in abundance (Fig. 1b). This distinct sphingolipid remodeling was further supported by RNA-seq analysis of TKI-treated and untreated FLT3-ITD$^+$ AML cells. Sphingolipid metabolism-associated genes in the Gene Ontology category were differentially expressed between the two groups (Fig. 1c). GSEA revealed that the sphingolipid signaling pathway was significantly upregulated in sorafenib-resistant MV4-11 cells than in parental cells (Fig. 1d). To identify the specific sphingolipids associated with sorafenib resistance, we utilized LC-MS-based targeted metabolomics in Molm13 cells to quantify key metabolites in the sphingolipid pathway, including sphingomyelin, ceramide, sphingosine, and S1P (Fig. 1e). Our findings revealed elevated levels of sphingosine and sphingosine 1-phosphate following sorafenib treatment compared to those in parental cells (Fig. 1f–h). Collectively, these results suggest that long-term FLT3 inhibition resulted in a broad reprogramming of sphingolipid metabolism.

SPHK1/S1P axis is activated upon prolonged exposure to sorafenib

To validate the clinical relevance of sphingolipid metabolism, we used the KM Plotter database to assess the prognostic value of 16 key sphingolipid metabolic genes in patients with AML. High expression of SPHK1, SPHK2, KDSR, SGMS1, SGPL1, and CERK correlated with poor overall survival (Fig. 2a and Table S5). We then performed qRT-PCR analysis to quantify the expression of these genes in sorafenib-exposed Molm13 and MV4-11 cell lines as well as in unexposed cells. SPHK1 was the only sphingolipid metabolic gene significantly upregulated in both sorafenib-treated cell lines relative to untreated cells (Fig. 2b, c). Western blot analysis confirmed the upregulation of SPHK1 in the two sorafenib-exposed cell lines (Fig. 2d). Given that SPHK1 catalyzes the phosphorylation of sphingosine to S1P, these results were consistent with the LC-MS results of sorafenib-treated Molm13 cells (Fig. 1h). Subsequently, the association between SPHK1/S1P levels and prolonged sorafenib exposure was investigated in FLT3-ITD$^+$ AML patient samples. We observed higher levels of SPHK1 and S1P in all six relapsed/refractory FLT3-ITD$^+$ AML patients who received at least 28 days of sorafenib treatment relative to baseline samples collected at the time of diagnosis. Further analysis confirmed absence of this up-regulation after the first two cycles of chemotherapy without sorafenib treatments (Fig. 2e). These results provide evidence of an enhanced dependence on SPHK1/S1P signaling during long-term FLT3 inhibitor exposure in FLT3-ITD$^+$ AML cells.

β-catenin serves as the downstream effector of SPHK1/S1P to counteract FLT3 inhibition

We further explored the mechanisms underlying SPHK1-mediated AML pathogenesis using TCGA data. Patients with AML were divided into high- and low-expression subgroups based on the median expression of SPHK1. GSEA revealed that gene signatures associated with LSCs, Wnt/β-catenin signaling, and its downstream

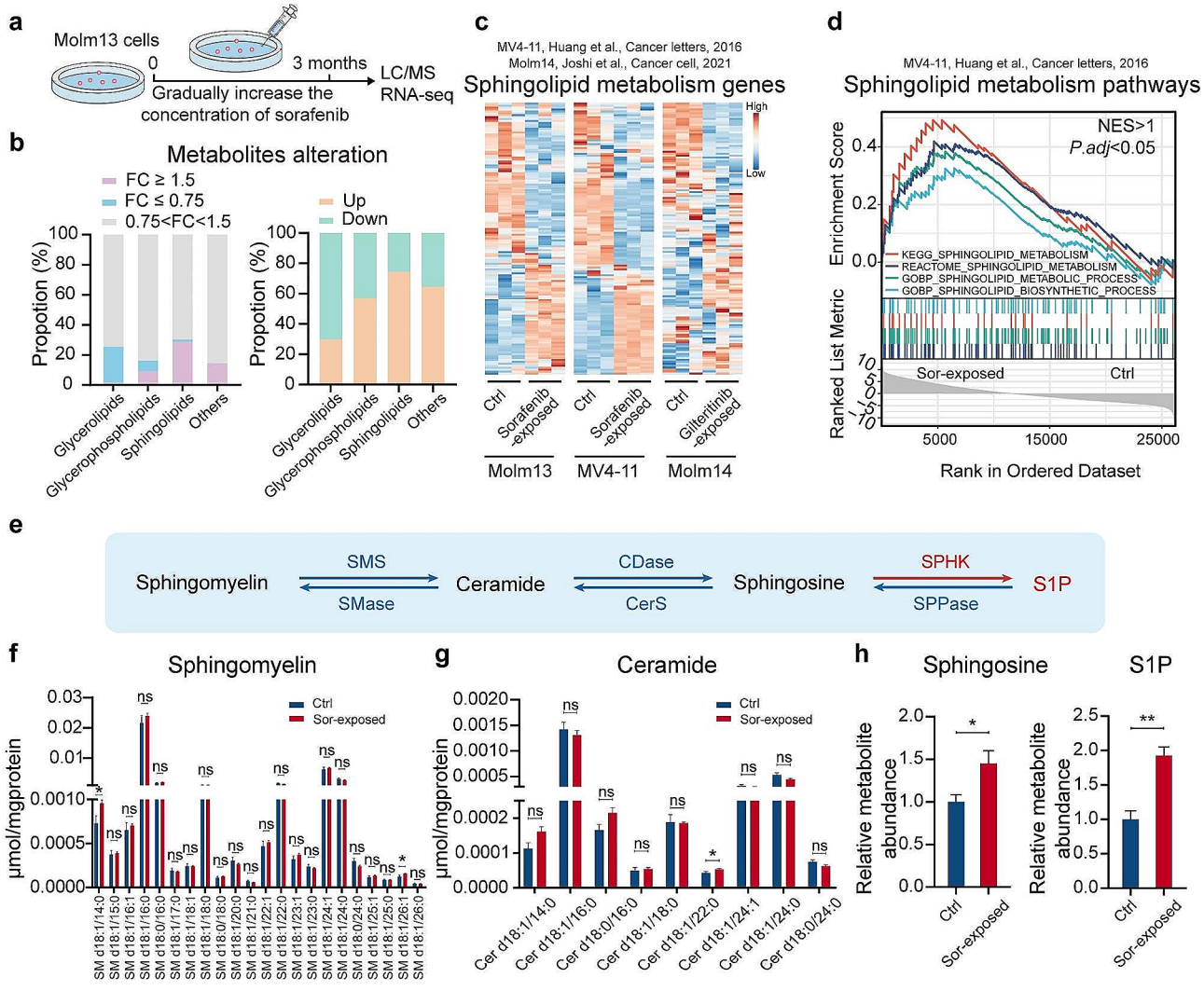

Fig. 1 FLT3-ITD$^+$ AML cells exhibit changes in sphingolipid metabolism changes upon long-term FLT3 inhibition. (**a**) Experimental scheme. Exposure of Molm13 cells to gradually increasing concentrations of sorafenib for 3 months, followed by LC/MS and RNA-seq analysis. (**b**) Lipidomic profiles in sorafenib-exposed Molm13 cells revealed via LC-MS and expressed as fold-change (FC) compared to parental cells ($n = 4$ biological replicates). (**c**) Heatmap showing differentially expressed genes in the Gene Ontology category associated with sphingolipid metabolism in TKI resistant FLT3-ITD$^+$ AML cells. (**d**) GSEA of the upregulated genes signatures in sorafenib resistant MV4-11 cells (normalized enrichment score [NES] > 1; *adj.P* < 0.05). (**e**) Schematic of the four major sphingolipid metabolites. (**f**–**h**) Lipidomic analysis of parental and sorafenib-exposed Molm13 cells via LC-MS-based targeted metabolomics ($n = 4$ biological replicates). Data are presented as the mean ± SEM. Ctrl, control; Sor, sorafenib; ns, non-significant difference.*$p < 0.05$

target myc were upregulated in FLT3-mutated AML patients with high SPHK1 expression (Fig. 3a). The activation of β-catenin has been shown to promote FLT3-ITD$^+$ AML progression and reduce TKI sensitivity by supporting the maintenance of LSCs [17, 26, 27]. Our qRT-PCR results showed a positive correlation between CTNNB1 and SPHK1 expression in AML patients (Fig. 3b), with an approximately 2.6-fold increase in CTNNB1 expression observed in patients versus healthy donors (Fig. 3c). Furthermore, patients with high CTNNB1 expression were stratified into groups with poor OS (Fig. S1). Therefore, we decided to focus on β-catenin as a driver of resistance.

Treatment with the SPHK inhibitor SKI-II decreased intracellular S1P levels (Fig. 3d) and induced a dose- and time-dependent inhibition of β-catenin and its target genes, including c-Myc, CD44, and survivin (Fig. 3e, f and Fig. S2a), thereby promoting the apoptosis of Molm13 and MV4-11 cells (Fig. 3g and Fig. S2b). However, the addition of exogenous S1P partially decreased SKI-II-induced β-catenin inhibition (Fig. 3h) and reduced SKI-II-induced apoptosis in both cell lines (Fig. 3g and Fig. S2b). These findings demonstrated that β-catenin serves as a downstream mediator of SPHK1/S1P to protect cells against FLT3 inhibitors.

SPHK1/S1P upregulates β-catenin via the S1P2 receptor

Activated SPHK1 can translocate from the cytoplasm to the plasma membrane, where the generated S1P is

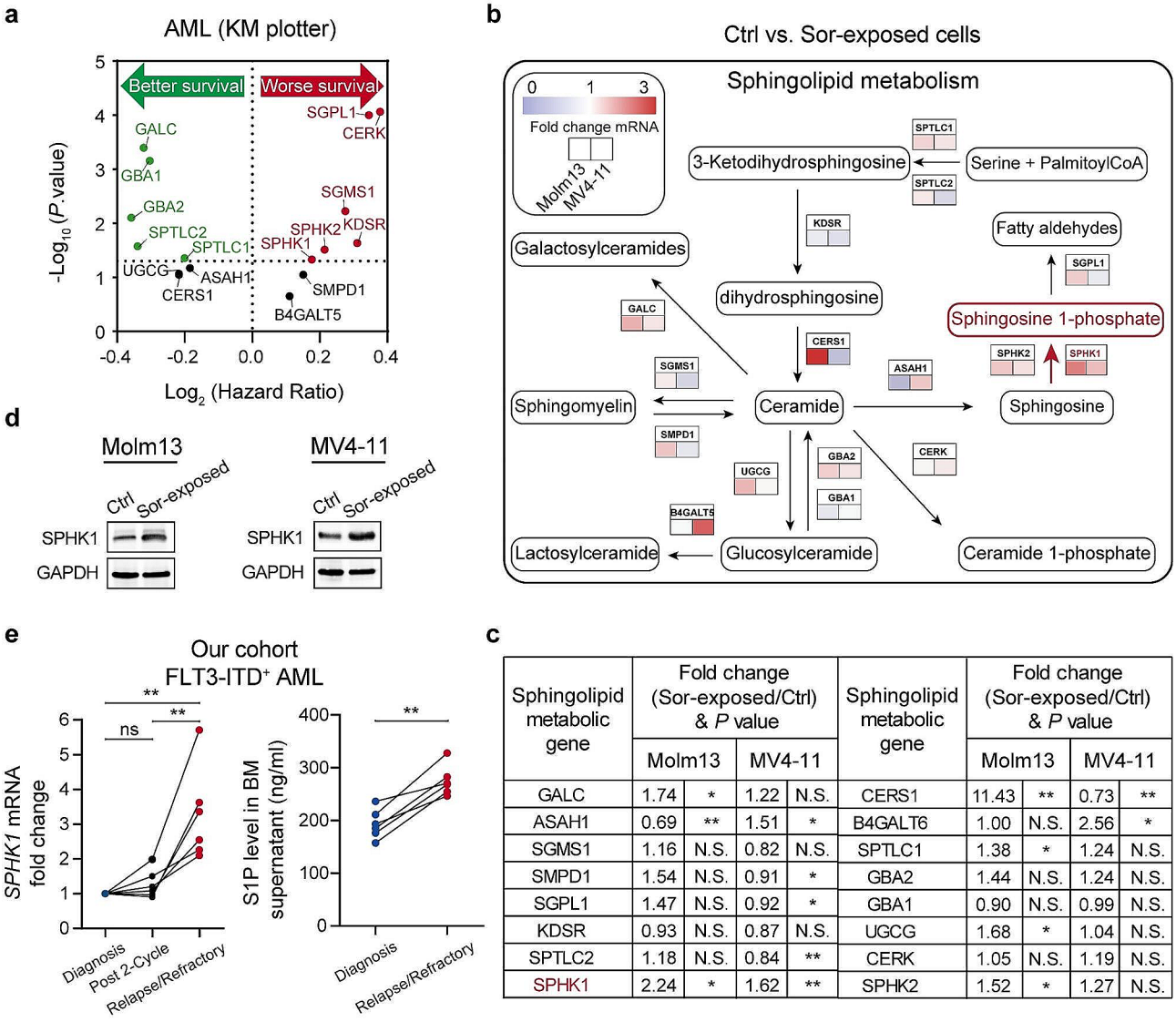

c

Sphingolipid metabolic gene	Fold change (Sor-exposed/Ctrl) & *P* value				Sphingolipid metabolic gene	Fold change (Sor-exposed/Ctrl) & *P* value			
	Molm13		MV4-11			Molm13		MV4-11	
GALC	1.74	*	1.22	N.S.	CERS1	11.43	**	0.73	**
ASAH1	0.69	**	1.51	*	B4GALT6	1.00	N.S.	2.56	*
SGMS1	1.16	N.S.	0.82	N.S.	SPTLC1	1.38	*	1.24	N.S.
SMPD1	1.54	N.S.	0.91	*	GBA2	1.44	N.S.	1.24	N.S.
SGPL1	1.47	N.S.	0.92	*	GBA1	0.90	N.S.	0.99	N.S.
KDSR	0.93	N.S.	0.87	N.S.	UGCG	1.68	*	1.04	N.S.
SPTLC2	1.18	N.S.	0.84	**	CERK	1.05	N.S.	1.19	N.S.
SPHK1	2.24	*	1.62	**	SPHK2	1.52	*	1.27	N.S.

Fig. 2 Long-term sorafenib treatment upregulates the SPHK1/S1P axis in FLT3-ITD$^+$ AML cells. (**a**) Volcano plot illustrating the hazard ratio (Log_2) and P value ($-Log_{10}$) between overall survival and the expression of 16 sphingolipid metabolic genes in AML (KM Plotter database). Genes linked to poor prognosis are highlighted in red. (**b**) Metabolic network of the sphingolipid metabolic reactions, together with main metabolites and 16 selected sphingolipid metabolic genes. Expression heatmap of the 16 selected sphingolipid genes in sorafenib-exposed Molm13 and MV4-11 cells compared to in their parental cells. (**c**) Average fold change and statistical analysis of the expression of 16 sphingolipid metabolism genes between sorafenib-exposed cell lines and their parental cells. (**d**) Western blot analysis of SPHK1 expression in both sorafenib-treated (3 months) cell lines as compared to their parental cells. (**e**) qRT-PCR analysis of SPHK1 expression in BM mononuclear blasts and ELISA detection of S1P levels in BM supernatant ($n=6$, our cohort) from paired primary diagnosis, post 2-cycle of chemotherapy, and relapsed/refractory FLT3-ITD$^+$ AML patients. Data are presented as the mean ± SEM. Ctrl, control; Sor, sorafenib; N.S., non-significant difference.*$p<0.05$, **$p<0.01$

exported from cells and binds S1P receptors, thereby exerting downstream biological effects in an autocrine manner [28]. Among the five S1P receptors, S1P2–5 were predominantly expressed in FLT3-ITD$^+$ AML cell lines (Fig. 4a). Notably, S1P2 was the only receptor upregulated in both Molm13 and MV4-11 cell lines following prolonged sorafenib exposure (Fig. 4b). We analyzed TCGA data to explore the role of S1P1–5 receptors in AML. S1P2 showed the strongest correlation with SPHK1 expression (Fig. S3a), which we confirmed via qRT-PCR analysis of patient samples (Fig. 4c). Increased S1P2 expression was observed in newly diagnosed AML patients compared to that in healthy individuals, with further elevation in relapsed/refractory AML cases (Fig. 4d). Higher S1P2 levels were also found in intermediate and poor-risk AML cases than in those with favorable risk (Fig. S3b). Additionally, high S1P2 expression stratified FLT3-ITD$^+$ AML patients into a group with poor OS (Fig. 4e), suggesting that S1P2 is a potential biomarker for AML prognosis.

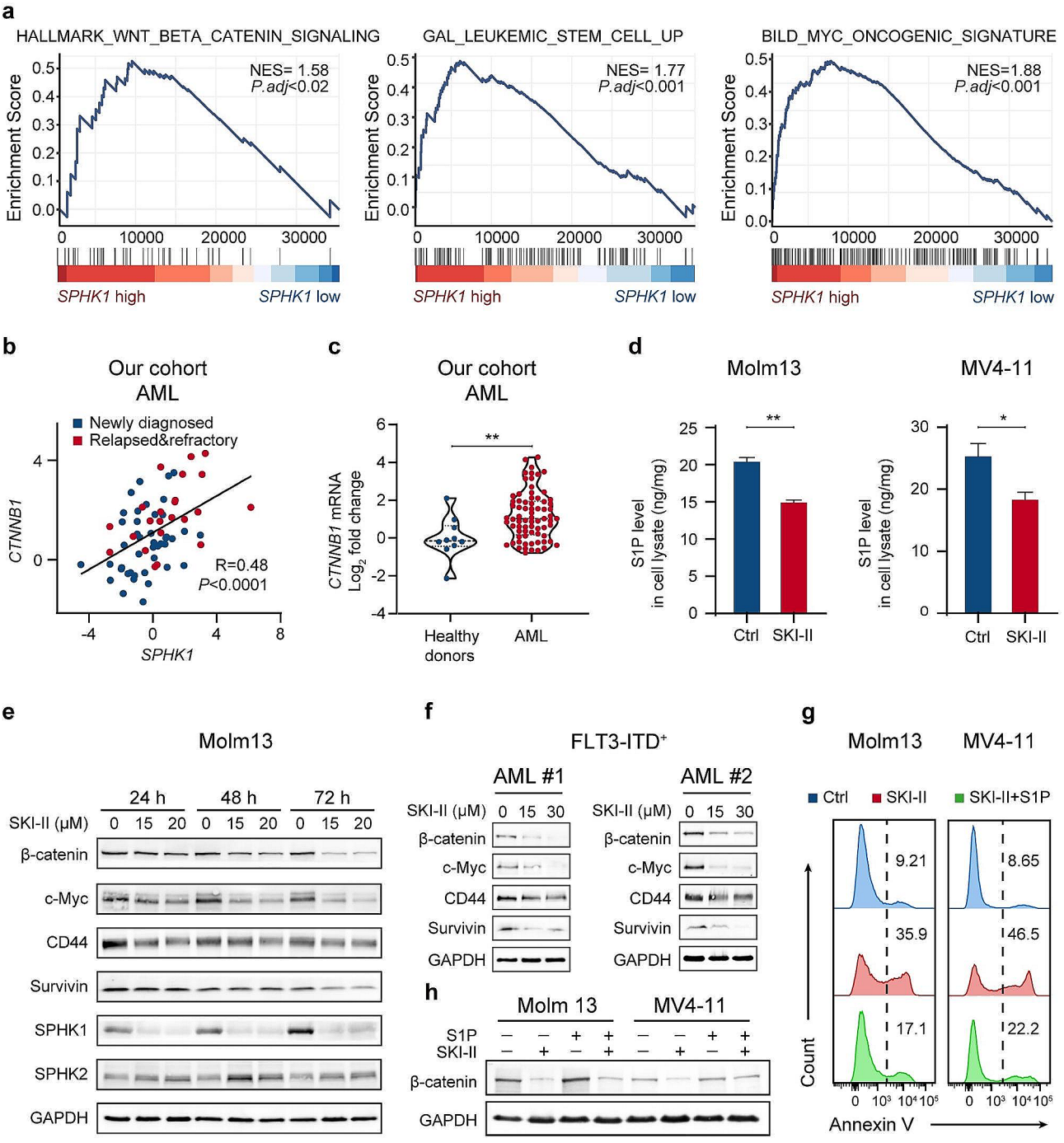

Fig. 3 SPHK1/S1P axis upregulates β-catenin signaling and maintains leukemia cell survival. (**a**) GSEA of the upregulated genes signatures in FLT3-mutated AML patients with high SPHK1 expression (NES > 1; *adj.P* < 0.05) from the TCGA cohort. (**b**) Pearson correlation between SPHK1 and CTNNB1 expression in AML patient samples determined via qRT-PCR ($n = 66$, our cohort). (**c**) qRT-PCR analysis of relative CTNNB1 expression in healthy donors ($n = 10$) and AML patients ($n = 66$) from our cohort. Values are shown as $\log_2$ fold-change relative to healthy donors. (**d**) ELISA detection of S1P levels in lysates from Molm13 and MV4-11 cells treated with SKI-II (20 μM) for 24 h. (**e**) Western blot analysis of Molm13 cells after treatment with the indicated concentrations of SKI-II for 24, 48, and 72 h. (**f**) Western blot analysis of primary FLT3-ITD$^+$ AML blasts treated with the indicated concentrations of SKI-II (48 h). (**g**) Apoptosis in Molm13 and MV4-11 cells pretreated with or without exogenous BSA-conjugated S1P (1 μM, added once every 3 h for 24 h) for 2 h, followed by treatment with SKI-II (25 μM) for 24 h. (**h**) Western blot analysis of Molm13 and MV4-11 cells treated with SKI-II (20 μM), S1P (1 μM), or both for 24 h. Data are presented as the mean ± SEM. Ctrl, control. *$p < 0.05$, **$p < 0.01$

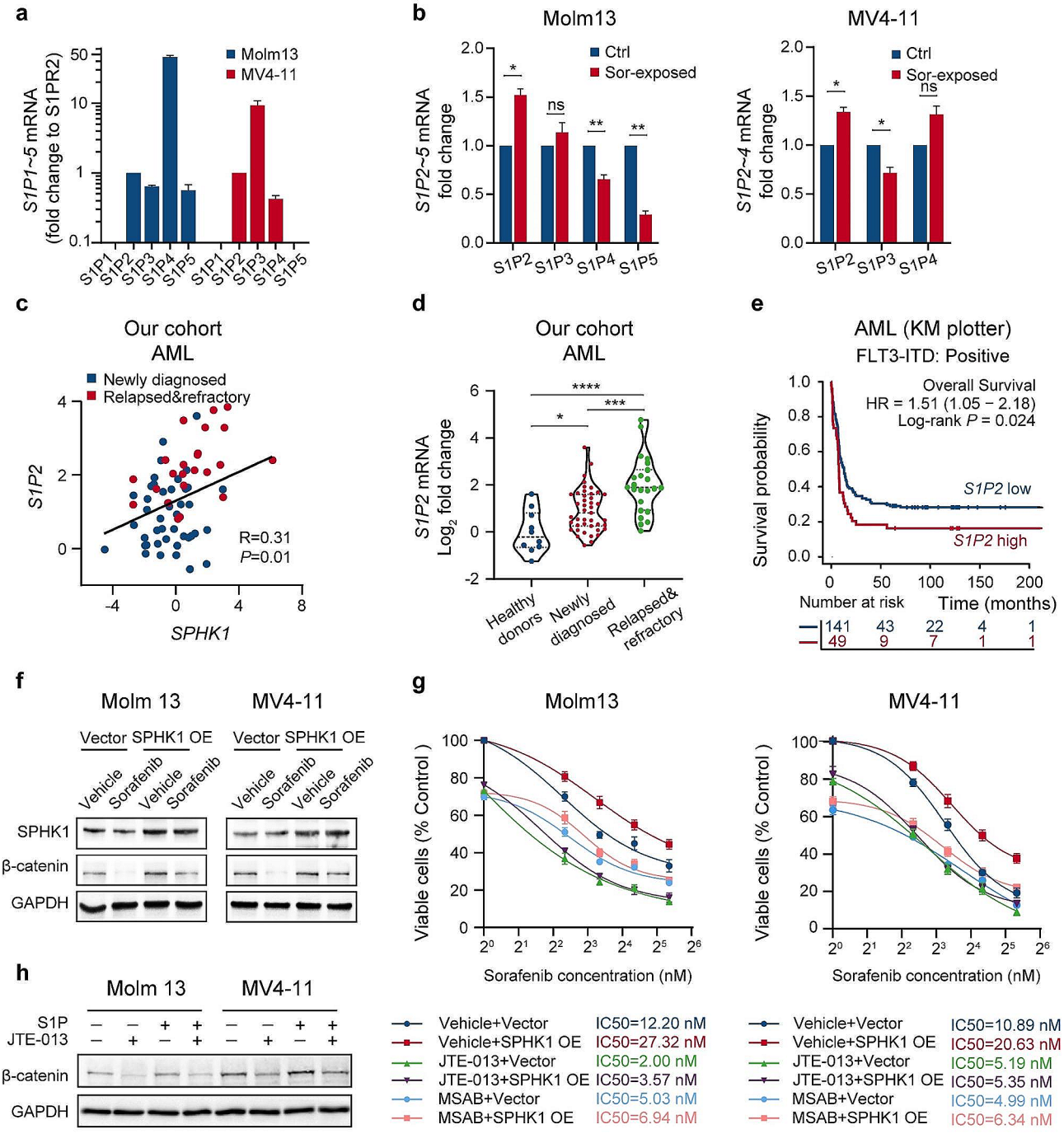

Fig. 4 SPHK1/S1P enhances β-catenin signaling via the S1P2 receptor. (**a**) qRT-PCR analysis of S1P1-5 expression in Molm13 and MV4-11 cells. (**b**) qRT-PCR analysis of S1P receptor expression in sorafenib-exposed cell lines and their parental cells. (**c**) Pearson correlation between S1P2 and SPHK1 expression in AML patient samples determined via qRT-PCR ($n=66$, our cohort). (**d**) qRT-PCR analysis of relative S1P2 expression in healthy donors ($n=10$), newly diagnosed AML patients ($n=43$), and relapsed/refractory AML patients ($n=23$) from our cohort. Values are shown as $\log_2$ fold-change relative to healthy donors. (**e**) Overall survival of FLT3-ITD$^+$ AML patients with high or low S1P2 expression ($n=190$, KM plotter database). (**f**) Molm13 and MV4-11 cells, transduced with empty vectors (Vector) or SPHK1-expressing vectors (SPHK1 OE), were treated with sorafenib (15 or 30 nM) for 24 h and subjected to western blot to detect the indicated proteins. (**g**) Molm13 and MV4-11 cells were transduced with Vector or SPHK1 OE and then treated with either the vehicle (dimethyl sulfoxide), JTE-013 (S1P2 inhibitor, 20 μM), or MSAB (β-catenin inhibitor, 3 μM), followed by culture with increasing doses of sorafenib for 24 h. Cell viability was measured using a CCK-8 assay. Median inhibitory concentration (IC50) values for sorafenib are shown at bottom. (**h**) Western blot analysis in Molm13 and MV4-11 cells treated with JTE-013 (20 μM), S1P (1 μM), or both for 24 h. Data are presented as the mean ± SEM. Ctrl, control; Sor, sorafenib; ns, non-significant difference. *$p<0.05$, **$p<0.01$, ***$p<0.001$, ****$p<0.0001$

Overexpression of SPHK1 increased β-catenin expression and protected Molm13 and MV4-11 cells from sorafenib-induced growth inhibition, which could be partially attenuated by the β-catenin inhibitor MSAB and the S1P2 inhibitor JTE-013 (Fig. 4f, g). Western blot analysis showed that JTE-013 treatment decreased β-catenin in both cell lines, while exogenous S1P increased β-catenin expression compared to that in controls and prevented S1P-induced β-catenin upregulation (Fig. 4h). Collectively, these findings suggest that SPHK1/S1P axis activates β-catenin to counteract FLT3 inhibitors via the S1P2 receptor.

Synergistic cytotoxicity of SPHK1 inhibition with FLT3 inhibitors in FLT3-ITD$^+$ AML cells

Using CRISPR screening data from the DepMap database, we identified SPHK1 as playing a crucial role in the survival of myeloid malignancies, as indicated by its notably low median chronos score (-0.197) across various cancer types (Fig. 5a). Subsequently, we investigated the synergistic effects of SPHK1 inhibition and FLT3 TKIs in FLT3-ITD$^+$ AML cells. CompuSyn analysis revealed significant synergistic cytotoxicity between sorafenib and SKI-II in Molm13 and MV4-11 cells (CI=0.55 and 0.29, respectively) (Fig. 5b, c). Similar results were observed in Molm13 and MV4-11 cells treated with quizartinib and SKI-II (CI=0.52 and 0.33, respectively) (Fig. 5d, e).

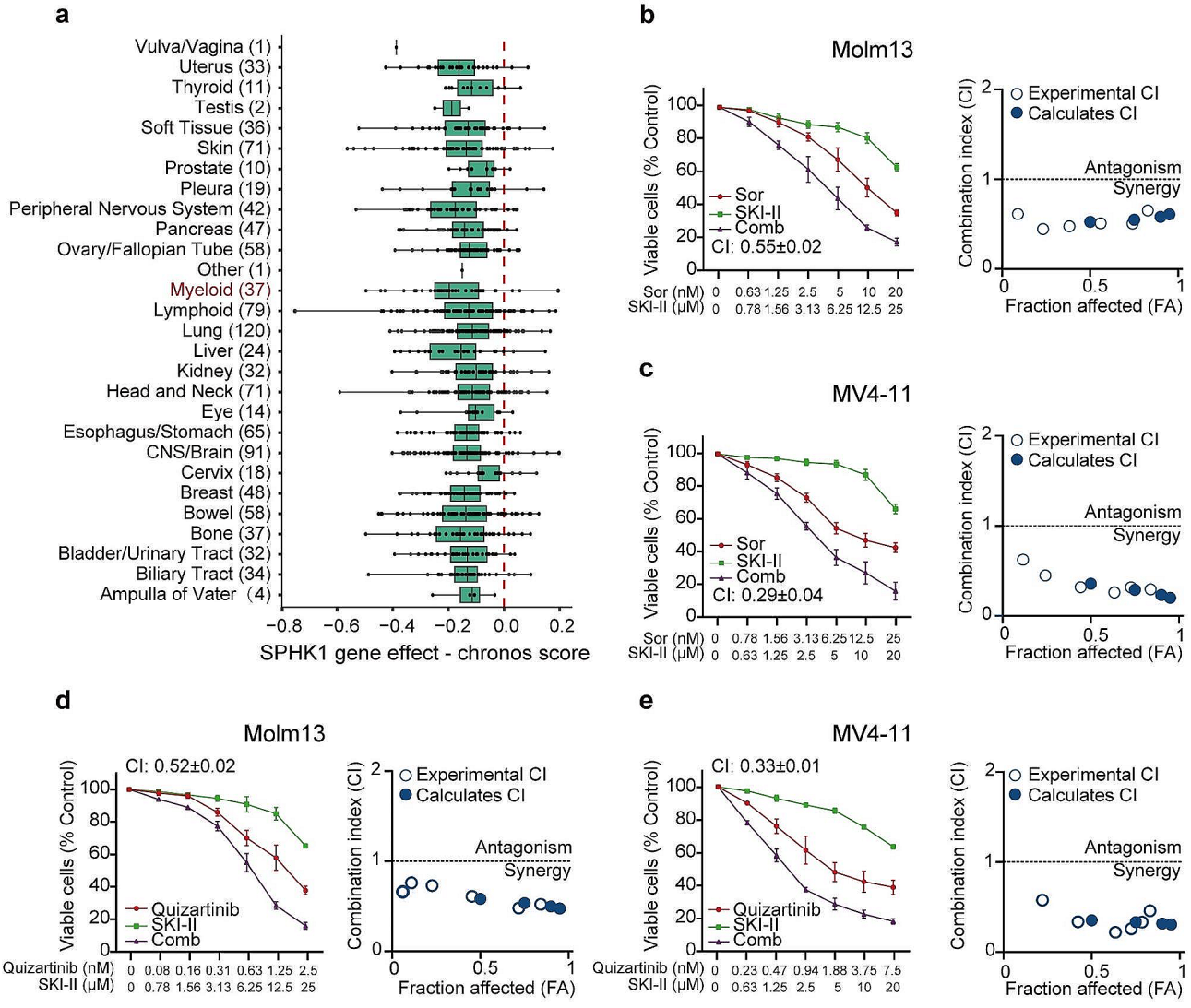

Fig. 5 Targeting SPHK1 impairs AML survival and synergizes with TKIs to suppress FLT3-ITD$^+$ AML cell proliferation. (**a**) Box plots visualize the cancer dependency on SPHK1 in different cancer lines (shown in the parenthesis) across different cancer types in the DepMap database. Cell lines with a chronos score < 0 (red line) exhibit SPHK1 dependency. Molm13 (**b**, **d**) and MV4-11 (**c**, **e**) cells were treated with FLT3 TKI (sorafenib or quizartinib), SKI-II, or both for 48 h. Cell viability was measured using an CCK-8 assay. Combinatorial Index (CI) blots are shown on the right. CI < 1 indicates a synergistic effect. Data are presented as the mean ± SEM. Ctrl, control; Sor, sorafenib; Comb, combination

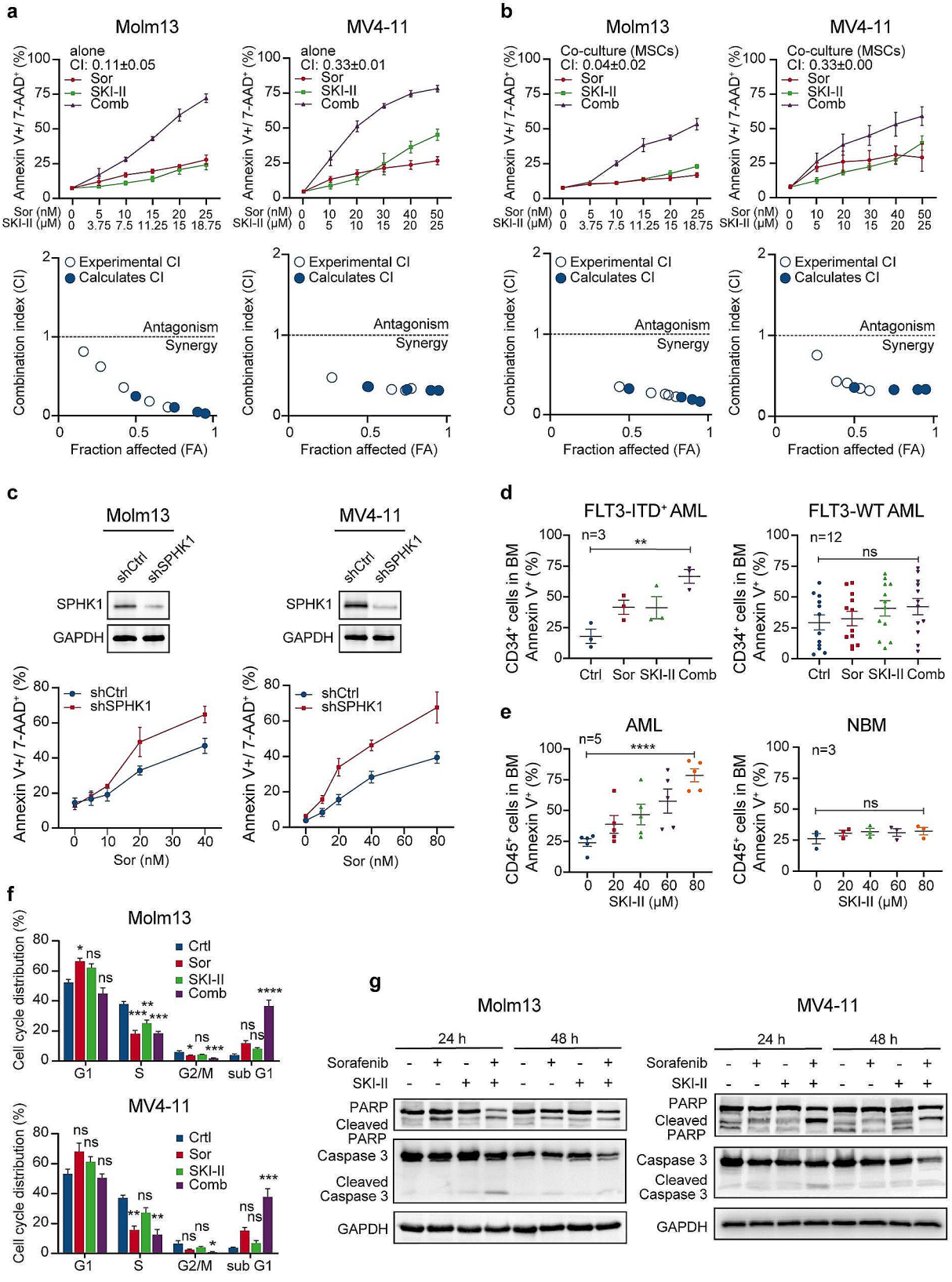

Fig. 6 (See legend on next page.)

(See figure on previous page.)

Fig. 6 SPHK1 inhibition synergistically enhances the TKI-induced apoptosis of FLT3-ITD$^+$ AML cells and CD34$^+$ AML stem cells. Apoptosis in Molm13 and MV4-11 cells without (**a**) or with (**b**) mesenchymal stem cells (MSCs) co-culture, following treatment with sorafenib, SKI-II, or both for 48 h. CI blots are shown at bottom. CI < 1 indicates a synergistic effect. (**c**) Apoptosis in Molm13 and MV4-11 cells expressing control shRNA (shCtrl) or SPHK1 shRNA (shSPHK1) upon sorafenib treatment for 48 h. SPHK1 depletion was confirmed via western blot. (**d**) Apoptosis of CD34$^+$ cells among FLT3-ITD$^+$ and FLT3-WT AML blasts treated with sorafenib (2 μM), SKI-II (30 μM), or both for 48 h. (**e**) Apoptosis of CD45$^+$ cells among AML and normal bone marrow (NBM) blasts treated with increasing doses of SKI-II, as indicated, for 48 h. (**f**) Cell cycle analysis of Molm13 or MV4-11 cells treated with sorafenib (15 or 30 nM), SKI-II (20 μM), or both for 24 h. (**g**) Levels of cleaved caspase 3 and PARP were analyzed by western blot in Molm13 and MV4-11 cells treated with sorafenib (15 or 30 nM), SKI-II (20 μM), or both for 24 and 48 h. Data are presented as the mean ± SEM. Ctrl, control; Sor, sorafenib; Comb, combination. *$p < 0.05$, **$p < 0.01$, ***$p < 0.001$, ****$p < 0.0001$

Conversely, no synergistic effects were observed in FLT3-WT AML HL60 and THP-1 cells (CI > 1) (Fig. S4). Collectively, these findings indicate that targeting SPHK1 could significantly enhance the leukemia-killing efficacy of TKIs in FLT3-ITD$^+$ AML.

Co-inhibition of SPHK1 and FLT3 synergistically induces apoptosis in FLT3-ITD$^+$ AML and CD34$^+$ cells

We treated FLT3-ITD$^+$ AML cells with sorafenib, SKI-II, or both and observed a marked synergistic induction of apoptosis in Molm13 and MV4-11 cells (CI = 0.11 and 0.33, respectively) (Fig. 6a), even when they were protected by co-culture with human bone marrow-derived mesenchymal stem cells (CI = 0.04 and 0.33, respectively) (Fig. 6b and Fig. S5). Similar results were obtained in Molm13 and MV4-11 cells upon treatment with quizartinib and SKI-II (CI = 0.33 and 0.25, respectively) (Fig. S6a). No synergy was detected in FLT3-WT AML cells following the combination treatment (CI > 1) (Fig. S6b). Molm13 and MV4-11 cells were transduced with lentiviral vectors expressing SPHK1 shRNA and then treated with sorafenib. SPHK1 knockdown enhanced sorafenib-induced apoptosis in these cells (Fig. 6c). Moreover, synergy was observed in CD34$^+$ and CD45$^+$ cells from FLT3-ITD$^+$ AML patients treated with sorafenib and SKI-II, whereas cells from FLT3-WT AML patients exhibited resistance to sorafenib, with no synergy observed upon combination treatment (Fig. 6d and Fig. S6c, d). Notably, SKI-II induced dose-dependent apoptosis in primary AML bulk cells. In contrast, either the drug alone or in combination therapy, as well as high concentrations of SKI-II, exhibited minimal effects on normal CD34$^+$ and CD45$^+$ cells from healthy donors (Fig. 6e and Fig. S6e).

Cell cycle analysis showed that the drug combination decreased the number of S and G2/M phase cells, while increasing that of cells in the sub-G1 phase (Fig. 6f and Fig. S6f), consistent with the growth inhibition and apoptosis induction described above. Accordingly, western blot analysis revealed elevated cleavage of apoptosis markers, including caspase 3 and PARP, following treatment with sorafenib and SKI-II in Molm13 and MV4-11 cells (Fig. 6g).

SPHK1 knockdown enhances the antileukemic activity of sorafenib against FLT3-mutated AML xenografts

To assess the impact of SPHK1 knockdown on sorafenib efficacy in FLT3-mutated AML in vivo, we transduced Molm13-GFP/Luc cells with lentiviral vectors expressing shCtrl or shSPHK1 and intravenously injected them into NCG mice (Fig. 7a). Administration of sorafenib modestly reduced the leukemia burden in mice grafted with cells expressing shSPHK1 compared to shCtrl, with significant effects observed on day 21, as demonstrated by in vivo imaging analysis (Fig. 7b, c). On day 14 post-treatment, BM and spleen samples were collected ($n = 3$/group). Sorafenib modestly decreased leukemia cell infiltration in the shSPHK1 group compared to the shCtrl group, as evidenced by reduced spleen sizes (Fig. 7d) and flow cytometric measurement of human CD45$^+$ cells in the tissues (Fig. 7e). Survival analysis revealed that mice treated with sorafenib had significantly improved median survival compared to controls (25 d vs. 17 d; $P < 0.001$), and SPHK1 knockdown further extended the survival benefit conferred by sorafenib (27 d; $P < 0.01$ vs. sorafenib alone; $P < 0.001$ vs. control) (Fig. 7f). These experiments suggest that SPHK1 knockdown enhances the antileukemic activity of sorafenib in vivo against FLT3-mutated AML.

Targeting β-catenin signaling via combination treatment

Next, we explored the effects of combined treatment on β-catenin and its downstream genes. Western blotting showed that SKI-II plus an FLT3 TKI (sorafenib or quizartinib) disrupted the expression of β-catenin and its downstream targets to a greater extent than monotherapy in Molm13, MV4-11 (Fig. 8a and Fig. S7a, b), and FLT3-ITD$^+$ AML samples (Fig. 8b). Similarly, while SPHK1 knockdown only modestly decreased the expression of β-catenin signaling factors, sorafenib treatment in combination further suppressed β-catenin expression (Fig. 8c). Immunofluorescence staining revealed that sorafenib and SKI-II in combination reduced the expression of total β-catenin and CD44 as well as β-catenin nuclear localization in Molm13 and MV4-11 cells (Fig. 8d and Fig. S7c), with the latter effect further confirmed via western blot (Fig. 8e). Taken together, these results indicate that co-inhibition of SPHK1 and FLT3 potently

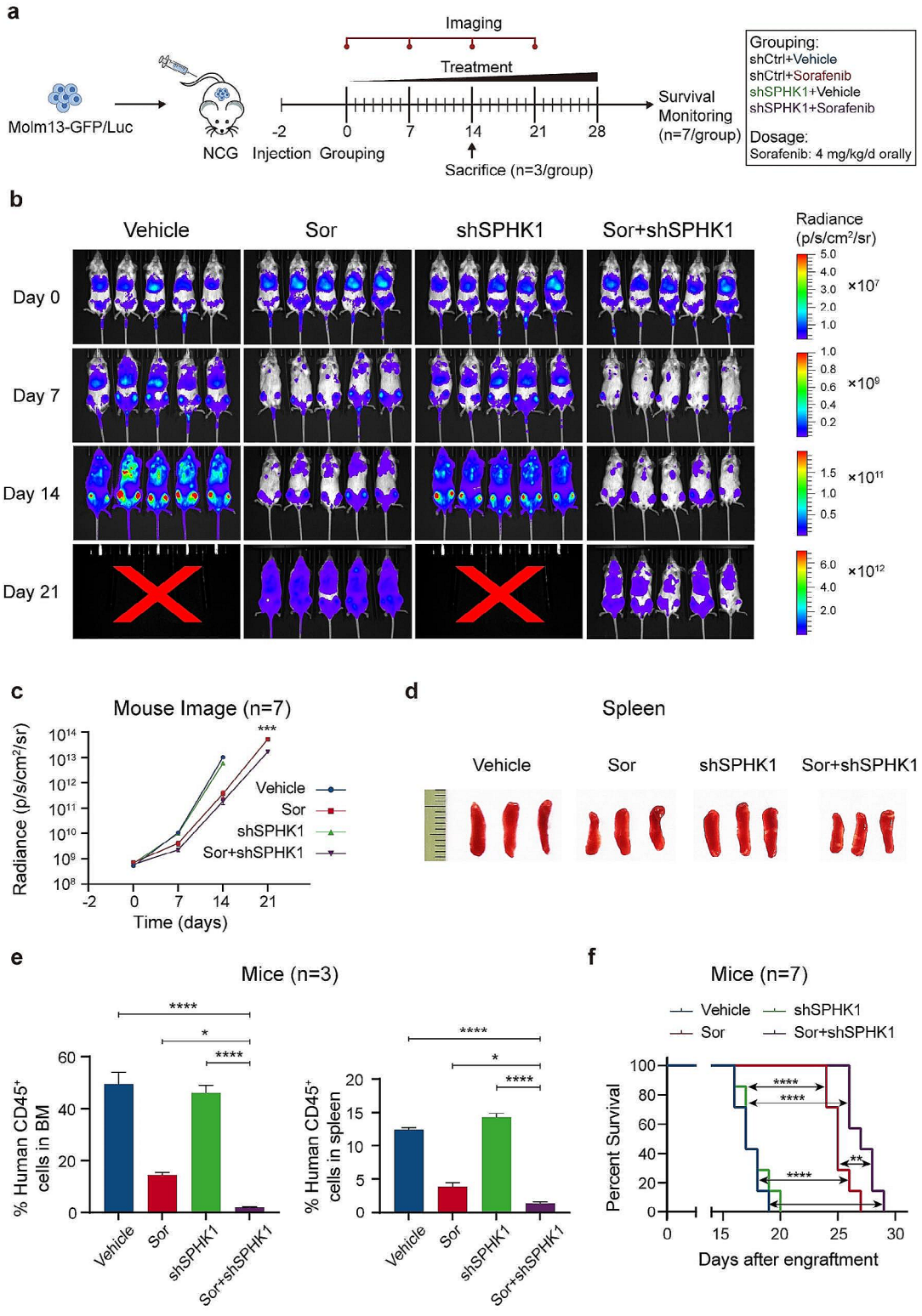

Fig. 7 SPHK1 knockdown enhances sorafenib activity in Molm13-GFP/Luc xenograft NCG mice. (**a**) Experimental scheme. NCG mice were injected intravenously with 5×10^5 Molm13-GFP/Luc cells expressing shCtrl or shSPHK1. After engraftment was confirmed, mice were treated daily with vehicle or sorafenib for 4 weeks. (**b**–**c**) Bioluminescent imaging (**b**) and quantification (**c**) at designated time points. (**d**) Spleen sizes of mice ($n = 3$/group). (**e**) Flow cytometric analysis of human CD45$^+$ leukemia cells in mouse BM and spleen after a 14-day treatment ($n = 3$/group). (**f**) Kaplan–Meier survival curve of mice ($n = 7$/group). Data are presented as the mean ± SEM. Sor, sorafenib; *$p < 0.05$, **$p < 0.01$, ****$p < 0.0001$

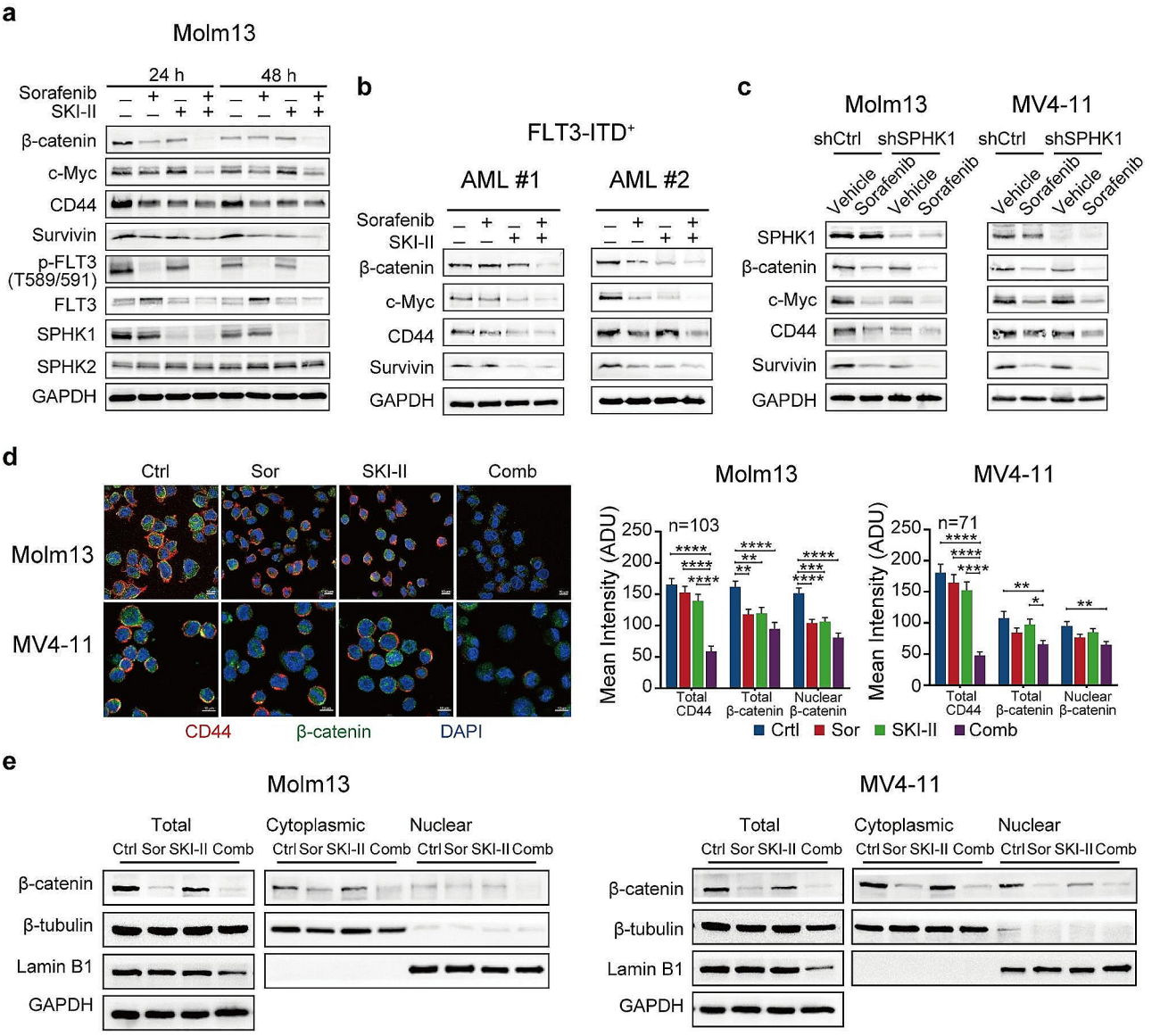

Fig. 8 Combined SPHK1 inhibitor and TKI treatment suppresses β-catenin signaling, reducing β-catenin nuclear localization. (**a**) Western blot analysis of Molm13 cells after treatment with sorafenib (15 nM), SKI-II (20 μM), or both for 24 and 48 h. (**b**) Western blot analysis of primary FLT3-ITD$^+$ AML blasts treated with sorafenib (2 μM), SKI-II (20 μM), or both for 48 h. (**c**) Western blot analysis of Molm13 and MV4-11 cells expressing shCtrl or shSPHK1 following sorafenib (15 or 30 nM) treatment for 24 h. (**d**) Confocal images and quantification of total CD44, total β-catenin, and nuclear β-catenin levels in Molm13 or MV4-11 cells treated with sorafenib (15 or 30 nM), SKI-II (20 μM), or both for 48 h. Scale bars indicate 10 μm. (**e**) β-catenin expression in total, cytoplasmic, and nuclear fractions was analyzed by western blot in Molm13 or MV4-11 cells treated with sorafenib (15 or 30 nM), SKI-II (20 μM), or both for 48 h, as determined via western blot. Data are presented as the mean ± SEM. Ctrl, control; Sor, sorafenib; Comb, combination. *$p < 0.05$, **$p < 0.01$, ***$p < 0.001$, ****$p < 0.0001$

inhibits β-catenin and its downstream targets, thereby inducing cell death in FLT3-ITD$^+$ AML cells.

Activation of the PP2A-GSK3β axis enhances β-catenin degradation

Protein phosphatase 2 A (PP2A) is a serine-threonine phosphatase that acts as a tumor suppressor [29]. PP2A has been shown to stimulate GSK3β activity by dephosphorylating it at Ser9 [30, 31]. Activated GSK3β functions as a protein kinase to promote β-catenin degradation via the proteasomal pathway [32]. Consequently, we investigated the impact of the PP2A-GSK3β axis on β-catenin signaling in the context of combination treatment.

PP2A is a heterotrimeric protein complex, with the C subunit regulating its catalytic activity. In FLT3-ITD$^+$ AML, impaired PP2A activity is associated with increased phosphorylation of Tyr307 on the PP2A-C subunit (p-PP2A-C) and increased expression of the

endogenous cancerous inhibitor of PP2A (CIP2A) [33]. Western blot revealed that co-inhibition of FLT3 (sorafenib or quizartinib) and SPHK1 (SKI-II or shRNA) synergistically reduced the expression of p-PP2A-C (Tyr307) and CIP2A, leading to almost complete suppression of p-GSK3β (Ser9) in Molm13 and MV4-11 cells (Fig. 9a–c). This reduction was correlated with the inhibition of β-catenin signaling, as previously described. Our results suggest that targeting SPHK1 activates PP2A by inhibiting p-PP2A-C and CIP2A, consequently promoting GSK3β dephosphorylation and leading to β-catenin downregulation.

To test this hypothesis, cells were pre-treated with the PP2A inhibitor okadaic acid. The inhibitory effects on p-GSK3β (Ser9) and β-catenin induced by SKI-II were effectively reversed (Fig. 9d). Furthermore, the SKI-II-induced β-catenin inhibition was completely reversed in cells pre-treated with GSK3β inhibitor TWS-119 (Fig. 9e), indicating that β-catenin inhibition is indeed mediated via PP2A-GSK3β activation. In summary, these results demonstrate that targeting SPHK1 activates PP2A to enhance GSK3β-mediated β-catenin inhibition.

Discussion

FLT3-ITD mutations induce constitutive tyrosine kinase activity and are associated with a poor prognosis. Although FLT3 TKIs show promise for the treatment of FLT3-ITD$^+$ AML, their clinical efficacy is transient [34, 35]. The inability of FLT3 TKIs to sustain the suppression of leukemic blasts suggests that compensatory survival signals are activated during prolonged FLT3 inhibition 5,7]. Therefore, it is imperative to elucidate the underlying mechanisms and identify novel targets for better treatment of FLT3-ITD$^+$ AML. In this study, we discovered that long-term sorafenib treatment induces robust sphingolipid metabolism dynamics and activates the SPHK1/S1P axis in FLT3-ITD$^+$ AML cells. SPHK1/S1P upregulates β-catenin via the S1P2 receptor to confer resistance against FLT3 inhibitors (Fig. 10). We further demonstrated that pharmacological or genetic inhibition of SPHK1 synergized with FLT3 inhibitors to suppress growth and induce apoptosis in FLT3-ITD$^+$ AML and CD34$^+$ blast cells in vitro, while also prolonging animal survival in vivo. The synergistic antileukemia activity of the combination was mediated via the inhibition

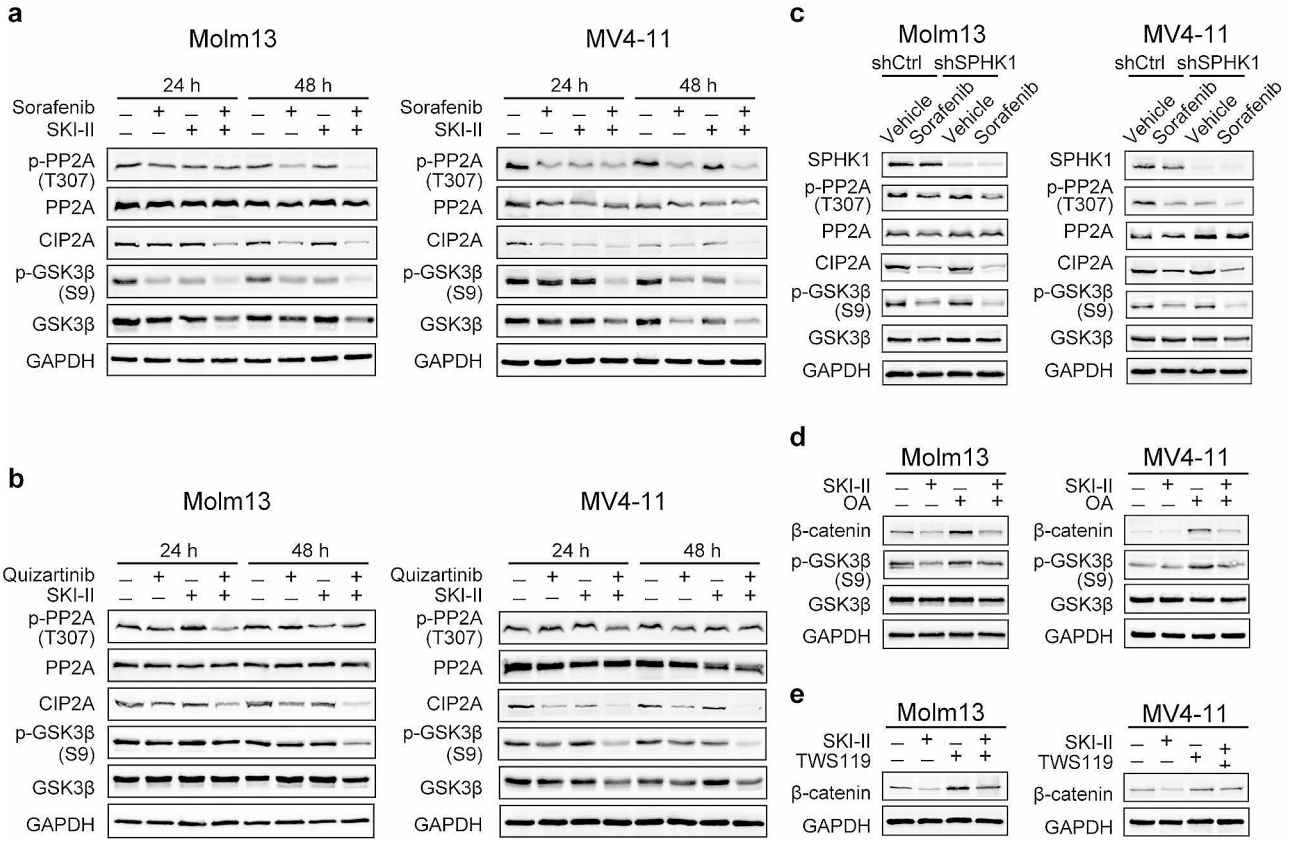

Fig. 9 Co-targeting SPHK1 and FLT3 stimulates β-catenin degradation via PP2A-GSK3β axis. (**a**–**b**) Western blot analysis of Molm13 and MV4-11 cells after treatment with (**a**) sorafenib (15 or 30 nM) or (**b**) quizartinib (1.2 or 2.4 nM) either alone or in combination with SKI-II (20 μM) for 24 and 48 h. (**c**) Western blot analysis of Molm13 and MV4-11 cells expressing shCtrl or shSPHK1 upon sorafenib (15 or 30 nM) treatment for 24 h. (**d**–**e**) Western blot analysis of Molm13 and MV4-11 cells after treatment with SKI-II (20 μM) in the absence/presence of (**d**) okadaic acid (OA, PP2A inhibitor; 10 nM) or (**e**) TWS119 (GSK3β inhibitor; 10 μM) for 24 h

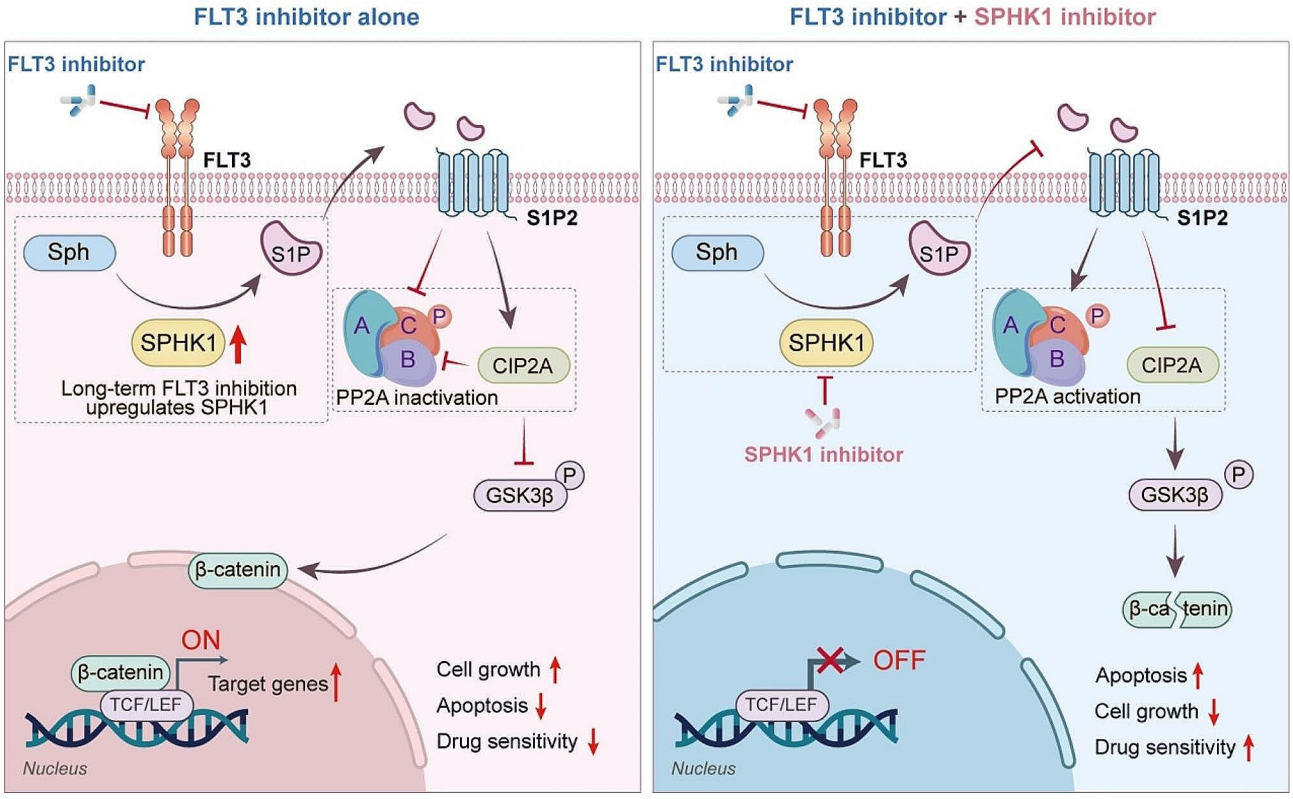

Fig. 10 Schematic model illustrating the mechanism of combined inhibition of FLT3 and SPHK1. When FLT3-ITD$^+$ AML cells are exposed to long-term FLT3 inhibitors, the SPHK1/S1P/S1P2 signaling is upregulated, leading to the inactivation of the PP2A-GSK3β axis. Subsequently, activated β-catenin translocates to the nucleus, facilitating the transcription of its target genes, thereby promoting the maintenance of FLT3-ITD$^+$ AML upon TKI treatment (left panel). However, concomitant targeting of SPHK1 and FLT3 signaling disrupts the inhibitory effect of SPHK1 on the PP2A-GSK3β axis and facilitates β-catenin degradation, thus significantly enhances FLT3 inhibitor-induced killing of leukemic cells (right panel)

of β-catenin through the activation of the PP2A-GSK3β pathway.

Studies have shown that S1P is upregulated in leukemia cells upon acquisition of gilteritinib resistance [25]. However, the association between dysregulated sphingolipid metabolism and FLT3 TKI resistance remains unclear. Based on lipidomic profiles and RNA-seq analysis, we demonstrated a notable enrichment of sphingolipid metabolism following prolonged exposure to sorafenib in FLT3-ITD$^+$ AML cells. SPHK1, a key enzyme catalyzing the synthesis of S1P, was the only sphingolipid metabolism-associated enzyme upregulated in both sorafenib-treated cell lines compared to untreated ones. Consistent with prior research demonstrating the potential of targeting SPHK1 to suppress AML cell proliferation [36–38], our findings confirmed that SPHK1 is essential for sustaining leukemia survival. SPHK1 inhibition potently enhanced the antileukemic activity of FLT3 inhibitors in FLT3-ITD$^+$ AML and CD34$^+$ blast cells in vitro, as well as facilitated superior animal survival in vivo.

Development of TKI resistance and subsequent disease relapse in FLT3-ITD$^+$ AML are driven by a small reservoir of quiescent LSCs [35]. Moreover, FLT3 signaling is known to stimulate the nuclear translocation and transcriptional activity of β-catenin [39]. Given the pivotal role of β-catenin in regulating both TKI sensitivity and LSC maintenance [20, 21, 26, 27], it represents a promising therapeutic target in FLT3-ITD$^+$ AML. In this study, we found that overactivated SPHK1/S1P signaling upregulated β-catenin expression and protected FLT3-ITD$^+$ AML cells from sorafenib treatment, while combination treatment with a β-catenin inhibitor resensitized leukemia cells to FLT3 TKIs.

The S1P2 receptor has emerged as a potential target for treating bone loss [40], inflammatory syndromes [41], brain disease [42], and various types of cancer [13, 43]. Reportedly, SPHK/S1P signaling promotes osteoblastogenesis by activating the p38-GSK3β-β-catenin pathway through the S1P2 receptor [40]. The elevated S1P2 expression we observed in relapsed/refractory AML patients compared to that in newly diagnosed patients suggests an important role for S1P2 in leukemia drug resistance. Furthermore, S1P2 was the only receptor upregulated in both FLT3-mutated AML cell lines after prolonged exposure to FLT3 inhibitors. Targeting S1P2 led to a reduction in the S1P-induced upregulation of

β-catenin, effectively counteracting the SPHK1 overexpression-induced resistance to sorafenib in FLT3-ITD$^+$ AML cells. Our results establish a crucial role for the S1P2 receptor in mediating SPHK1/S1P-induced β-catenin expression, thereby protecting FLT3-ITD$^+$ AML cells from TKI treatment.

However, the signaling pathways that mediate β-catenin degradation downstream of S1P2 remain unclear. Studies on chronic myeloid leukemia (CML) demonstrated that SPHK1/S1P/S1P2 activation increases BCR-ABL1 stability and induces resistance to imatinib through a PP2A-SHP1-dependent pathway [13]. Our mechanistic investigation showed that disruption of SPHK1/S1P and FLT3 signalings cooperatively abrogated the activity of β-catenin via activating the PP2A-GSK3β axis. PP2A is a tumor suppressor that inhibits kinase-driven intracellular survival pathways [29]. Phosphorylated PP2A-C (p-PP2A-C), the inactive form of PP2A, was overexpressed in FLT3-ITD$^+$ AML blasts compared to FLT3-WT blasts [44]. PP2A activation has been proposed as a novel approach for treating patients with FLT3-mutated AML [44–46]. Our results showed that the disruption of SPHK1 synergized with FLT3 TKIs to increase PP2A activity by reducing the expression of p-PP2A-C in FLT3-ITD$^+$ AML cells and patient samples. The activity of PP2A is also regulated by its endogenous inhibitor CIP2A [47]. Overexpression of CIP2A resulted in increased BCR-ABL1 activity and contributed to imatinib resistance by inhibiting PP2A in CML [48, 49]. Furthermore, high CIP2A expression correlates with FLT3-ITD mutations and indicates poor prognosis in AML with normal cytogenetics [50]. Therefore, CIP2A holds promise as a therapeutic target for enhancing TKI sensitivity in FLT3-ITD$^+$ AML cells. Consistently, our results suggest that the concurrent targeting of FLT3 and SPHK1 activates PP2A by inhibiting its suppressor CIP2A.

GSK-3β, a substrate for PP2A [30, 31], plays a significant role by phosphorylating β-catenin, facilitating its subsequent deactivation and proteasomal degradation. In contrast, non-phosphorylated β-catenin translocates into the nucleus and interacts with co-transcriptional regulator T-cell factor/lymphoid enhancer factor, subsequently activating the transcription of Wnt-targeted genes [32].

Recent evidence supports midostaurin and quizartinib as category 1 treatments according to NCCN guidelines for FLT3-positive AML [51]. Both agents affect the PP2A, GSK3β, and β-catenin pathways in FLT3-ITD$^+$ AML [39, 45, 52, 53]. Specifically, midostaurin inhibits nuclear β-catenin localization and reduces c-Myc and cyclin D1 levels [39], while loss-of-function mutations in GSK3 activate the Wnt/β-catenin pathway, contributing to quizartinib resistance [52, 53]. PP2A-activating drugs enhance quizartinib efficacy by inhibiting AKT and promoting GSK3β-mediated proteasomal degradation of c-Myc and Pim-1 [45]. Our study demonstrated that SPHK1 inhibition synergistically enhances sorafenib or quizartinib efficacy via PP2A-GSK3β activation and β-catenin degradation in FLT3-ITD$^+$ AML cells. Furthermore, sorafenib, midostaurin, and quizartinib exhibit distinct kinase inhibition profiles and modes of interaction with FLT3, leading to a spectrum of both distinct and overlapping resistance mechanisms [54]. FLT3 secondary mutations (TKD-D835/Y842/F691), compensatory pro-survival pathways, and epigenetic modifications are commonly observed in sorafenib and quizartinib resistance, whereas quizartinib resistance also involves cellular energetic and metabolic adaptations [54]. In contrast, midostaurin resistance primarily results from mutations linked to the RAS/MAPK pathway, alongside pro-survival mechanisms [54]. Our findings underscore dysregulated sphingolipid metabolism and an upregulated SPHK1/S1P axis following prolonged sorafenib exposure, a mechanism not yet reported for quizartinib or midostaurin. These findings provide a mechanistic rationale for targeting SPHK1/S1P/S1P2 signaling, particularly through downstream pro-survival factor β-catenin, as a promising strategy for AML treatment.

Conclusions

Our study revealed that prolonged exposure to sorafenib activates the SPHK1/S1P axis, leading to the upregulation of the pro-survival protein β-catenin. Furthermore, we showed synergistic effects of SPHK1 inhibition combined with FLT3 inhibitors on cell proliferation suppression and apoptosis by targeting PP2A/GSK3β/β-catenin signaling in FLT3-ITD$^+$ AML cells. Our results suggest that combination therapy targeting both SPHK1 and FLT3 holds promise for the treatment of FLT3-mutated AML.

Abbreviations

AML	Acute myeloid leukemia
TKI	Tyrosine kinase inhibitors
FLT3	FMS-like receptor tyrosine kinase-3
ITD	Internal tandem duplication
SPHK1	Sphingosine kinase 1
S1P	Sphingosine-1-phosphate
LSC	Leukemia stem cell
BM	Bone marrow
qRT-PCR	quantitative reverse transcription-polymerase chain reaction
KM	Kaplan–Meier
TCGA	The Cancer Genome Atlas
GSEA	Gene set enrichment analysis
ELISA	Enzyme-linked immunosorbent assay

Supplementary Information

The online version contains supplementary material available at https://doi.org/10.1186/s12964-024-01774-9.

Supplementary Material 1

Supplementary Material 2

Acknowledgements
The authors gratefully acknowledge the contributions of all fellows at the Nanfang Hospital for technical assistance. The authors thank all patients and their physicians for providing primary specimens for this study.

Author contributions
LJ contributed to the design and conduct of the experiments, data analysis, and preparation of the manuscript; YZ assisted with the animal experiments and data analysis. FL and YH assisted with gene knockdown experiments and were involved in analyzing the data; YZ, BY, JC, and PY collected primary samples; LJ, JN, YJ, and QW performed the bioinformatics analysis; XJ conceived and designed the overall concept and reviewed and edited the manuscript. All authors read and approved the final version of the manuscript.

Funding
This work was supported by the National Natural Science Foundation of China (82170165) and GuangDong Basic and Applied Basic Research Foundation (2023A1515012401 and 2021A1515011437).
Author information.
Ling Jiang and Yu Zhao contributed equally to this work.

Data availability
LC-MS data is provided within the supplementary information files. Other data analyzed during this study are available from the corresponding author upon request. Public datasets analyzed during this study are available in GEO (https://www.ncbi.nlm.nih.gov/geo/) or The Cancer Genome Atlas (https://portal.gdc.cancer.gov/) database.

Declarations

Ethics approval and consent to participate
This study was approved by the Medical Ethics Committee of Nanfang Hospital (Approval Number: NFEC-2023-568). Informed consent was obtained from all subjects involved in the study.

Consent for publication
All authors read and approved the final manuscript.

Competing interests
The authors declare no competing interests.

Author details
[1]Department of Hematology, Nanfang Hospital, Southern Medical University, Guangzhou, China
[2]Department of Hematology, The Third Affiliated Hospital of Southern Medical University, Guangzhou, China
[3]School of Medicine, Zhengzhou University, Zhengzhou, China

Received: 1 May 2024 / Accepted: 1 August 2024
Published online: 07 August 2024

References

1. Ley TJ, Miller C, Ding L, Raphael BJ, Mungall AJ, Robertson AG, Hoadley K, Triche TJ, Laird PW, Baty JD, et al. Genomic and epigenomic landscapes of adult de novo acute myeloid leukemia. N Engl J Med. 2013;368(22):2059–74.
2. Choudhary C, Olsen JV, Brandts C, Cox J, Reddy PNG, Böhmer FD, Gerke V, Schmidt-Arras D-E, Berdel WE, Müller-Tidow C, et al. Mislocalized activation of oncogenic RTKs switches downstream signaling outcomes. Mol Cell. 2009;36(2):326–39.
3. Gebru MT, Wang H-G. Therapeutic targeting of FLT3 and associated drug resistance in acute myeloid leukemia. J Hematol Oncol. 2020;13(1):155.
4. Yang X, Sexauer A, Levis M. Bone marrow stroma-mediated resistance to FLT3 inhibitors in FLT3-ITD AML is mediated by persistent activation of extracellular regulated kinase. Br J Haematol. 2014;164(1):61–72.
5. Piloto O, Wright M, Brown P, Kim K-T, Levis M, Small D. Prolonged exposure to FLT3 inhibitors leads to resistance via activation of parallel signaling pathways. Blood. 2007;109(4):1643–52.
6. McMahon CM, Ferng T, Canaani J, Wang ES, Morrissette JJD, Eastburn DJ, Pellegrino M, Durruthy-Durruthy R, Watt CD, Asthana S, et al. Clonal selection with RAS Pathway Activation mediates secondary clinical resistance to selective FLT3 inhibition in Acute myeloid leukemia. Cancer Discov. 2019;9(8):1050–63.
7. Park IK, Mundy-Bosse B, Whitman SP, Zhang X, Warner SL, Bearss DJ, Blum W, Marcucci G, Caligiuri MA. Receptor tyrosine kinase Axl is required for resistance of leukemic cells to FLT3-targeted therapy in acute myeloid leukemia. Leukemia. 2015;29(12):2382–9.
8. Hannun YA, Obeid LM. Sphingolipids and their metabolism in physiology and disease. Nat Rev Mol Cell Biol. 2018;19(3):175–91.
9. Ogretmen B. Sphingolipid metabolism in cancer signalling and therapy. Nat Rev Cancer. 2018;18(1):33–50.
10. Zheng X, Li W, Ren L, Liu J, Pang X, Chen X, Kang D, Wang J, Du G. The sphingosine kinase-1/sphingosine-1-phosphate axis in cancer: potential target for anticancer therapy. Pharmacol Ther. 2019;195:85–99.
11. Cuvillier O, Pirianov G, Kleuser B, Vanek PG, Coso OA, Gutkind S, Spiegel S. Suppression of ceramide-mediated programmed cell death by sphingosine-1-phosphate. Nature. 1996;381(6585):800–3.
12. Cartier A, Hla T. Sphingosine 1-phosphate: lipid signaling in pathology and therapy. Science 2019, 366(6463).
13. Salas A, Ponnusamy S, Senkal CE, Meyers-Needham M, Selvam SP, Saddoughi SA, Apohan E, Sentelle RD, Smith C, Gault CR, et al. Sphingosine kinase-1 and sphingosine 1-phosphate receptor 2 mediate Bcr-Abl1 stability and drug resistance by modulation of protein phosphatase 2A. Blood. 2011;117(22):5941–52.
14. Rosa R, Marciano R, Malapelle U, Formisano L, Nappi L, D'Amato C, D'Amato V, Damiano V, Marfè G, Del Vecchio S, et al. Sphingosine kinase 1 overexpression contributes to cetuximab resistance in human colorectal cancer models. Clin Cancer Res. 2013;19(1):138–47.
15. Alkafaas SS, Elsalahaty MI, Ismail DF, Radwan MA, Elkafas SS, Loutfy SA, Elshazli RM, Baazaoui N, Ahmed AE, Hafez W, et al. The emerging roles of sphingosine 1-phosphate and SphK1 in cancer resistance: a promising therapeutic target. Cancer Cell Int. 2024;24(1):89.
16. Liu J, Xiao Q, Xiao J, Niu C, Li Y, Zhang X, Zhou Z, Shu G, Yin G. Wnt/β-catenin signalling: function, biological mechanisms, and therapeutic opportunities. Signal Transduct Target Ther. 2022;7(1):3.
17. Tickenbrock L, Schwäble J, Wiedehage M, Steffen B, Sargin B, Choudhary C, Brandts C, Berdel WE, Müller-Tidow C, Serve H. Flt3 tandem duplication mutations cooperate with wnt signaling in leukemic signal transduction. Blood. 2005;105(9):3699–706.
18. Wang Y, Krivtsov AV, Sinha AU, North TE, Goessling W, Feng Z, Zon LI, Armstrong SA. The Wnt/beta-catenin pathway is required for the development of leukemia stem cells in AML. Science. 2010;327(5973):1650–3.
19. Dietrich PA, Yang C, Leung HHL, Lynch JR, Gonzales E, Liu B, Haber M, Norris MD, Wang J, Wang JY. GPR84 sustains aberrant β-catenin signaling in leukemic stem cells for maintenance of MLL leukemogenesis. Blood. 2014;124(22):3284–94.
20. Perry JM, Tao F, Roy A, Lin T, He XC, Chen S, Lu X, Nemechek J, Ruan L, Yu X, et al. Overcoming Wnt-β-catenin dependent anticancer therapy resistance in leukaemia stem cells. Nat Cell Biol. 2020;22(6):689–700.
21. Jiang X, Mak PY, Mu H, Tao W, Mak DH, Kornblau S, Zhang Q, Ruvolo P, Burks JK, Zhang W, et al. Disruption of Wnt/β-Catenin exerts Antileukemia Activity and synergizes with FLT3 inhibition in FLT3-Mutant Acute myeloid leukemia. Clin Cancer Res. 2018;24(10):2417–29.
22. Liu H, Zhang C-X, Ma Y, He H-W, Wang J-P, Shao R-G. SphK1 inhibitor SKI II inhibits the proliferation of human hepatoma HepG2 cells via the Wnt5A/β-catenin signaling pathway. Life Sci. 2016;151:23–9.
23. Lam SM, Zhang C, Wang Z, Ni Z, Zhang S, Yang S, Huang X, Mo L, Li J, Lee B, et al. A multi-omics investigation of the composition and function of extracellular vesicles along the temporal trajectory of COVID-19. Nat Metab. 2021;3(7):909–22.
24. Huang A, Ju H-Q, Liu K, Zhan G, Liu D, Wen S, Garcia-Manero G, Huang P, Hu Y. Metabolic alterations and drug sensitivity of tyrosine kinase inhibitor resistant leukemia cells with a FLT3/ITD mutation. Cancer Lett. 2016;377(2):149–57.
25. Joshi SK, Nechiporuk T, Bottomly D, Piehowski PD, Reisz JA, Pittsenbarger J, Kaempf A, Gosline SJC, Wang Y-T, Hansen JR et al. The AML microenvironment catalyzes a stepwise evolution to gilteritinib resistance. Cancer Cell 2021, 39(7).

26. Zhang B, Li M, McDonald T, Holyoake TL, Moon RT, Campana D, Shultz L, Bhatia R. Microenvironmental protection of CML stem and progenitor cells from tyrosine kinase inhibitors through N-cadherin and Wnt-β-catenin signaling. Blood. 2013;121(10):1824–38.
27. Jiang J, Griffin JD. Wnt/β-catenin pathway modulates the sensitivity of the mutant FLT3 receptor kinase inhibitors in a GSK-3β dependent manner. Genes Cancer. 2010;1(2):164–76.
28. Spiegel S, Milstien S. Sphingosine 1-phosphate, a key cell signaling molecule. J Biol Chem. 2002;277(29):25851–4.
29. Stanford SM, Bottini N. Targeting protein phosphatases in cancer immunotherapy and autoimmune disorders. Nat Rev Drug Discov. 2023;22(4):273–94.
30. Elgendy M, Cirò M, Hosseini A, Weiszmann J, Mazzarella L, Ferrari E, Cazzoli R, Curigliano G, DeCensi A, Bonanni B et al. Combination of Hypoglycemia and Metformin impairs Tumor metabolic plasticity and growth by modulating the PP2A-GSK3β-MCL-1 Axis. Cancer Cell 2019, 35(5).
31. Lambrecht C, Libbrecht L, Sagaert X, Pauwels P, Hoorne Y, Crowther J, Louis JV, Sents W, Sablina A, Janssens V. Loss of protein phosphatase 2A regulatory subunit B56δ promotes spontaneous tumorigenesis in vivo. Oncogene. 2018;37(4):544–52.
32. Stamos JL, Weis WI. The β-catenin destruction complex. Cold Spring Harb Perspect Biol. 2013;5(1):a007898.
33. Cristóbal I, Garcia-Orti L, Cirauqui C, Alonso MM, Calasanz MJ, Odero MD. PP2A impaired activity is a common event in acute myeloid leukemia and its activation by forskolin has a potent anti-leukemic effect. Leukemia. 2011;25(4):606–14.
34. Ma HS, Greenblatt SM, Shirley CM, Duffield AS, Bruner JK, Li L, Nguyen B, Jung E, Aplan PD, Ghiaur G, et al. All-trans retinoic acid synergizes with FLT3 inhibition to eliminate FLT3/ITD + leukemia stem cells in vitro and in vivo. Blood. 2016;127(23):2867–78.
35. Anderson NR, Sheth V, Li H, Harris MW, Qiu S, Crossman DK, Kumar H, Agarwal P, Nagasawa T, Paterson AJ, et al. Microenvironmental CXCL12 deletion enhances Flt3-ITD acute myeloid leukemia stem cell response to therapy by reducing p38 MAPK signaling. Leukemia. 2023;37(3):560–70.
36. Powell JA, Lewis AC, Zhu W, Toubia J, Pitman MR, Wallington-Beddoe CT, Moretti PAB, Iarossi D, Samaraweera SE, Cummings N, et al. Targeting sphingosine kinase 1 induces MCL1-dependent cell death in acute myeloid leukemia. Blood. 2017;129(6):771–82.
37. Yang L, Weng W, Sun Z-X, Fu X-J, Ma J, Zhuang W-F. SphK1 inhibitor II (SKI-II) inhibits acute myelogenous leukemia cell growth in vitro and in vivo. Biochem Biophys Res Commun. 2015;460(4):903–8.
38. Li Y, Gao Y, Liang B, Nie W, Zhao L, Wang L. Combined effects on leukemia cell growth by targeting sphingosine kinase 1 and sirtuin 1 signaling. Exp Ther Med. 2020;20(6):262.
39. Kajiguchi T, Chung EJ, Lee S, Stine A, Kiyoi H, Naoe T, Levis MJ, Neckers L, Trepel JB. FLT3 regulates beta-catenin tyrosine phosphorylation, nuclear localization, and transcriptional activity in acute myeloid leukemia cells. Leukemia. 2007;21(12):2476–84.
40. Weske S, Vaidya M, Reese A, von Wnuck Lipinski K, Keul P, Bayer JK, Fischer JW, Flögel U, Nelsen J, Epple M, et al. Targeting sphingosine-1-phosphate lyase as an anabolic therapy for bone loss. Nat Med. 2018;24(5):667–78.
41. Thibaut MM, Bindels LB. Crosstalk between bile acid-activated receptors and microbiome in entero-hepatic inflammation. Trends Mol Med. 2022;28(3):223–36.
42. van Echten-Deckert G. The role of sphingosine 1-phosphate metabolism in brain health and disease. Pharmacol Ther. 2023;244:108381.
43. Zeng Z, Ma C, Chen K, Jiang M, Vasu R, Liu R, Zhao Y, Zhang H. Roles of G protein-coupled receptors (GPCRs) in gastrointestinal cancers: Focus on Sphingosine 1-Shosphate receptors, angiotensin II receptors, and estrogen-related GPCRs. Cells 2021, 10(11).
44. Smith AM, Dun MD, Lee EM, Harrison C, Kahl R, Flanagan H, Panicker N, Mashkani B, Don AS, Morris J, et al. Activation of protein phosphatase 2A in FLT3 + acute myeloid leukemia cells enhances the cytotoxicity of FLT3 tyrosine kinase inhibitors. Oncotarget. 2016;7(30):47465–78.
45. Scarpa M, Singh P, Bailey CM, Lee JK, Kapoor S, Lapidus RG, Niyongere S, Sangodkar J, Wang Y, Perrotti D, et al. PP2A-activating drugs enhance FLT3 inhibitor efficacy through AKT inhibition-dependent GSK-3β-Mediated c-Myc and Pim-1 proteasomal degradation. Mol Cancer Ther. 2021;20(4):676–90.
46. Peris I, Romero-Murillo S, Martínez-Balsalobre E, Farrington CC, Arriazu E, Marcotegui N, Jiménez-Muñoz M, Alburquerque-Prieto C, Torres-López A, Fresquet V, et al. Activation of the PP2A-B56α heterocomplex synergizes with venetoclax therapies in AML through BCL2 and MCL1 modulation. Blood. 2023;141(9):1047–59.
47. Fujiki H, Sueoka E, Watanabe T, Komori A, Suganuma M. Cancer progression by the okadaic acid class of tumor promoters and endogenous protein inhibitors of PP2A, SET and CIP2A. J Cancer Res Clin Oncol 2023.
48. Lucas CM, Harris RJ, Giannoudis A, Copland M, Slupsky JR, Clark RE. Cancerous inhibitor of PP2A (CIP2A) at diagnosis of chronic myeloid leukemia is a critical determinant of disease progression. Blood. 2011;117(24):6660–8.
49. Lucas CM, Harris RJ, Holcroft AK, Scott LJ, Carmell N, McDonald E, Polydoros F, Clark RE. Second generation tyrosine kinase inhibitors prevent disease progression in high-risk (high CIP2A) chronic myeloid leukaemia patients. Leukemia. 2015;29(7):1514–23.
50. Lucas CM, Scott LJ, Carmell N, Holcroft AK, Hills RK, Burnett AK, Clark RE. CIP2A- and SETBP1-mediated PP2A inhibition reveals AKT S473 phosphorylation to be a new biomarker in AML. Blood Adv. 2018;2(9):964–8.
51. National Comprehensive Cancer Network (NCCN). NCCN Clinical Practice Guidelines in Oncology (NCCN Guidelines®): Acute Myeloid Leukemia. Version 2.2024. https://www.nccn.org/guidelines/guidelines-detail?category=1&id=1411
52. Hou P, Wu C, Wang Y, Qi R, Bhavanasi D, Zuo Z, Dos Santos C, Chen S, Chen Y, Zheng H, et al. A genome-wide CRISPR screen identifies genes critical for resistance to FLT3 inhibitor AC220. Cancer Res. 2017;77(16):4402–13.
53. Solovey M, Wang Y, Michel C, Metzeler KH, Herold T, Göthert JR, Ellenrieder V, Hessmann E, Gattenlöhner S, Neubauer A, et al. Nuclear factor of activated T-cells, NFATC1, governs FLT3ITD-driven hematopoietic stem cell transformation and a poor prognosis in AML. J Hematol Oncol. 2019;12(1):72.
54. Abdel-Aziz AK, Dokla EME, Saadeldin MK. FLT3 inhibitors and novel therapeutic strategies to reverse AML resistance: an updated comprehensive review. Crit Rev Oncol Hematol. 2023;191:104139.

Publisher's Note